ALASKA GEOBOTANY CENTER DATA REPORT

AGC 24-02

GROUND-BASED BIOMASS, LAI, & NDVI MEASUREMENTS, DEADHORSE, ALASKA

PRELIMINARY ANALYSES OF RELATIONSHIPS OF LAI AND NDVI TO BIOMASS AND SITE FACTORS ALONG A SITE-MOISTURE GRADIENT

DONALD A. WALKER, AMY L. BREEN, HELGA BÜLTMANN, HOWARD EPSTEIN, OLIVIA HOBGOOD, KELCY KENT, EMILY WATSON-COOK

EDITED BY D. A. WALKER AND J. L. PEIRCE

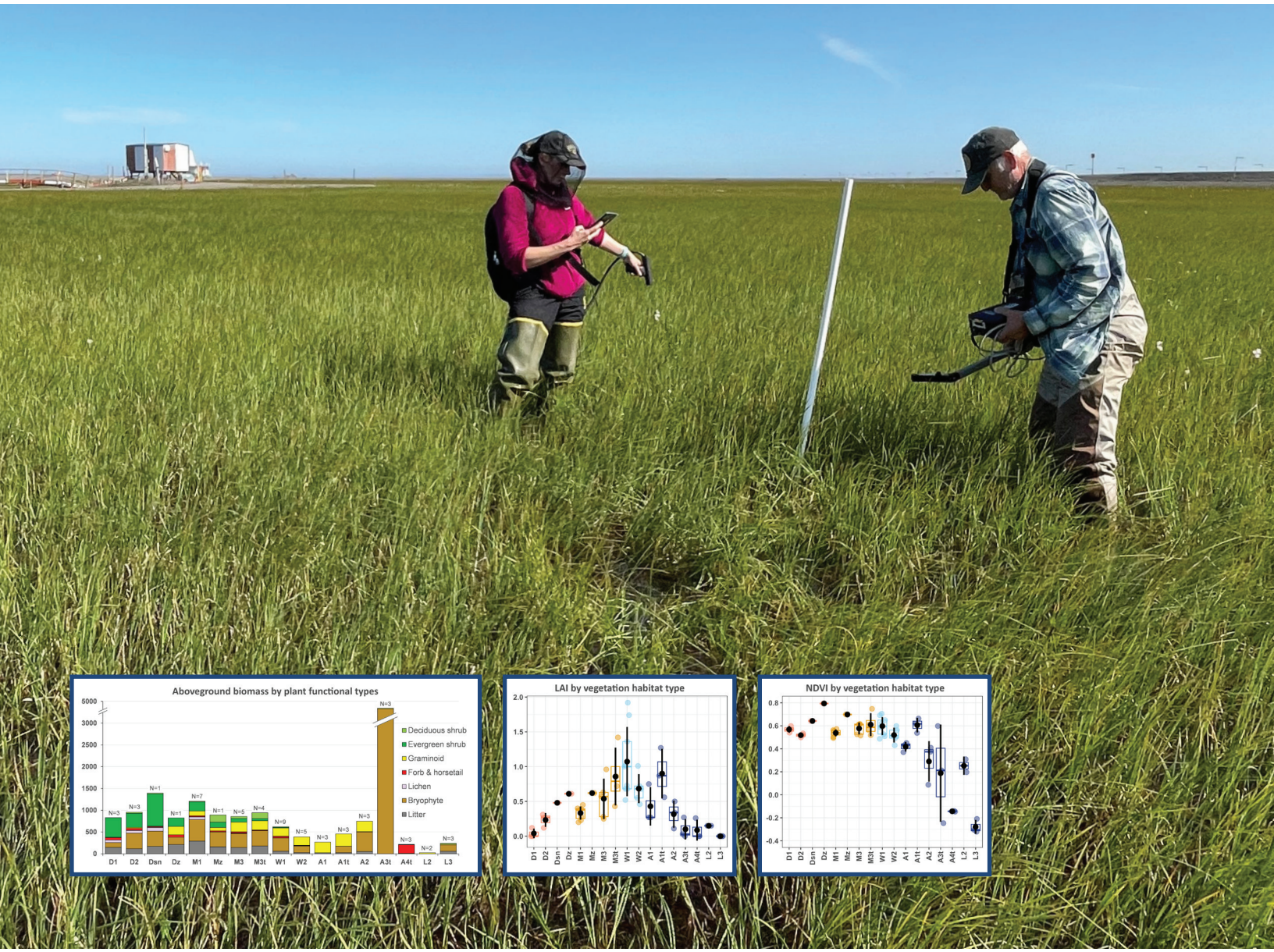

DECEMBER 2024

A PUBLICATION OF THE ALASKA GEOBOTANY CENTER 24-02

INSTITUTE OF ARCTIC BIOLOGY, UNIVERSITY OF ALASKA FAIRBANKS

GROUND-BASED BIOMASS, LAI, & NDVI MEASUREMENTS, DEADHORSE, ALASKA

PRELIMINARY ANALYSES OF RELATIONSHIPS OF LAI AND NDVI TO BIOMASS AND SITE FACTORS ALONG A SITE-MOISTURE GRADIENT

ALASKA GEOBOTANY CENTER DATA REPORT 24-02 :: DECEMBER 2024

Edited by Donald A. Walker and Jana L. Peirce

TABLE OF CONTENTS

CONTRIBUTORS

AMY L. BREEN, PHD
Institute of Arctic Biology & International Arctic Research Center, University of Alaska Fairbanks

HELGA BÜLTMANN, PHD
University of Münster, Germany

HOWARD EPSTEIN, PHD
Department of Environmental Sciences, University of Virginia

OLIVIA HOBGOOD
Alaska Geobotany Center, Institute of Arctic Biology and Department of Biology and Wildlife, University of Alaska Fairbanks

KELCY KENT, PHD
Department of Environmental Sciences, University of Virginia

DONALD A. WALKER, PHD
Alaska Geobotany Center, Institute of Arctic Biology and Department of Biology and Wildlife, University of Alaska Fairbanks

EMILY WATSON-COOK
Alaska Geobotany Center, Institute of Arctic Biology and Department of Biology and Wildlife, University of Alaska Fairbanks

Acknowledgments

Principal funding for this research is provided by the National Science Foundation (NSF) Navigating the New Arctic: Landscape evolution and adapting to change in ice-rich permafrost systems (NNA-IRPS) project (RISE Award 1928237). Support for the participation of Howard Epstein and Kelcy Kent was provided by NSF grants to the University of Virginia (Awards 2022639, 1721030). We also thank Batelle Arctic Research Operations and Arctic Oilfield Hotel for their logistical support, and the North Slope Borough for allowing us to do research on their lands.

How to cite this volume

Walker, D. A., Breen, A. L., Bültmann, H., Epstein, H. E., Hobgood, O., Kent, K., and Watson-Cook, E. 2024. Ground-based biomass, LAI, and NDVI measurements, Deadhorse, Alaska: Preliminary analyses of relationships of LAI and NDVI to biomass and site factors along a site-moisture gradient. AGC Data Report 24-02. Alaska Geobotany Center, University of Alaska Fairbanks, Fairbanks, Alaska, USA.

On the cover

Kelcy Kent and Skip Walker measure NDVI and LAI along Transect 4 at the Airport site (credit: Amy Breen). Inset figures (from left)**:** Trends along the site moisture gradient for aboveground biomass, LAI and NDVI.

1 Introduction

Measurements of biomass, leaf-area index (LAI), and Normalized Difference Vegetation Index (NDVI) were obtained from permanent vegetation plots representative of common vegetation types at study sites near Deadhorse in Prudhoe Bay, Alaska, which are part of the NSF-funded project, Navigating the New Arctic: Landscape evolution and adapting to change in ice-rich permafrost systems (NNA-IRPS) (figure 1).

Numerous characteristics of Arctic vegetation, including biomass, productivity, leaf-area, chlorophyll content, and fractional cover of vegetation are routinely assessed using ground-level and satellite-based spectral vegetation indices. NDVI is the most widely used spectral index, and is calculated as follows:

$$NDVI = (NIR - R)/(NIR + R),$$

where R and NIR stand for the spectral reflectance values in the red (visible) and near-infrared regions of the spectrum.

The data were collected to help assess the relationships between satellite-derived spectral data and ground-level measurements of vegetation and site factors. Such comparisons are necessary because measurement of LAI and NDVI in the Arctic are affected by a wide variety of unique environment- and instrument-related factors (e.g., Shippert et al. 1995, Asner et al. 1998; Stow et al. 2004; Hope et al. 2005; Buchhorn et al. 2013, 2016a; Raynolds et al. 2011, 2016, Myers-Smith et al. 2015, Frost et al. 2022, Heijmans, et al. 2022, Bergstedt et al. 2023, Jespersen et al. 2023).

The focus here is on the variation of biomass, LAI, and NDVI across the site-moisture gradient in non-acidic tundra at the boundary between Bioclimate Subzones C and D (CAVM Team 2003), or the approximate transitional band between the High and Low Arctic (Bliss 1997), where the zonal vegetation is currently predominantly graminoid, prostrate dwarf-shrub, moss tundra with few erect shrubs. This report complements earlier studies that focused on trends in biomass, LAI, and NDVI in mesic (zonal) vegetation across the full Arctic summer temperature gradient in North America and Europe (Raynolds et al. 2006, Epstein et al. 2008, 2021, Bhatt et al. 2010).

Site-moisture status is probably the most important factor to consider regarding variation in vegetation productivity in the Prudhoe Bay region and other flat tundra wetlands where the water table is largely controlled by the presence of near-surface permafrost (Raynolds et al. 2016). The flat thaw-lake plains are characterized by extensive areas of ice-wedge polygons with high percentages of wet and aquatic tundra. Additionally, since the early 1990s, small thermokarst thaw ponds, many with large amounts of aquatic vegetation (Watson-Cook 2022), have increased dramatically over much of the northern Alaska (Jorgenson et al. 2006, 2022; Raynolds et al. 2014; Kanevskiy et al. 2017, 2022; Frost et al. 2022).

Biomass, LAI and NDVI data were collected from permanent vegetation plots at the Natural Ice-Rich Permafrost Observatory (NIRPO) site where there are extensive plot-based and map data that portray the surficial geology, landforms, permafrost, soils and vegetation across the full local site-moisture gradient (Walker et al. 2023). LAI and NDVI data were also collected from the nearby Colleen and Airport roadside disturbance study sites (Walker et al. 2015, 2016). These data are presented without analysis because of the lack of biomass data at the roadside sites.

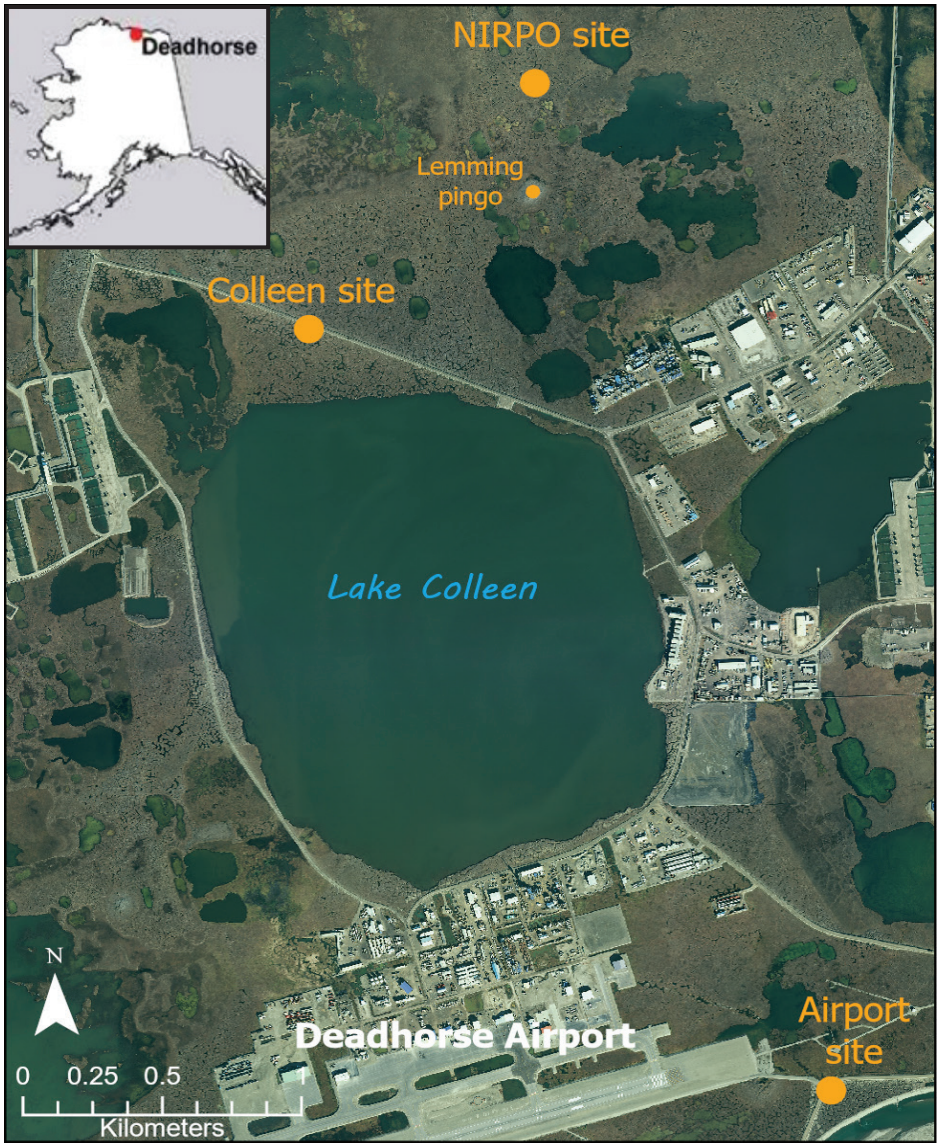

Figure 1. *Locations of NIRPO, Colleen and Airport study sites near Deadhorse, Alaska, in the vicinity of the airport and other service area infrastructure. Credit: Martha Raynolds.*

2 Methods

2.1 Study areas

Ground-based measurements of LAI and NDVI were obtained during 19-20 July 2023 from permanent vegetation plots at the Natural Ice-Rich Permafrost Observatory (NIRPO), Colleen site, and Airport site, near Deadhorse, Alaska (Figure 1).

2.1.1 NIRPO plots

The 59 NIRPO 1 x 1 m permanent vegetation plots are located within in the approximately 88 ha NIRPO site within the larger NIRPO-Jorgenson-Colleen (NJC) study area (Figure 2a); 45 plots are in the vicinity of research transects T6, T7, T8, and T9, and 14 plots are in the vicinity of Lemming Pingo (Figure 2b).

The locations of the NIRPO plots were chosen to be representatives of a full range of dry, moist, wet, and aquatic vegetation habitats encountered along transects T6, T7, T8, T9, and the Lemming Pingo vicinity within three surficial geology units described by Rawlinson (1993) and associated landforms (Figure 2, Table 1).

Forty-four plots were sampled in 2021, including 35 moist to wet terrestrial plots (21-01 to 21-35) and nine aquatic plots in ice-wedge thermokarst ponds (21A-22, 26, 27, 28, 29, 27, 35, 38, 40). Fifteen plots were sampled in 2022, including 8 dry plots (22-01–06, 22-13, and 22-14 on Lemming Pingo), one moist bird mound on Transect 8 (22-15), and 6 aquatic plots in lakes and ponds near Lemming Pingo (22-07 to 22-12). The methods of vegetation and environmental sampling were described in previous AGC data reports (Walker et al. 2022a, 2023).

2.1.1.1 Plot characterization

The legend codes used in figures characterizing the NIRPO plots throughout this report are defined in Table 1. The surficial geology codes refer to Quaternary age deposits described by Rawlinson (1993). The corresponding landforms refer to the landscape features associated with the surficial geology units. These include residual surfaces, lakes and ponds, drained thaw-lake basins (ice-poor and ice-rich), and pingos.

Surficial features correspond in part to "landforms" in the Geobotanical Atlas of the Prudhoe Bay Region (Everett 1980) and include patterned-ground features (e.g., frost boils, types of ice-wedge polygons, hum-

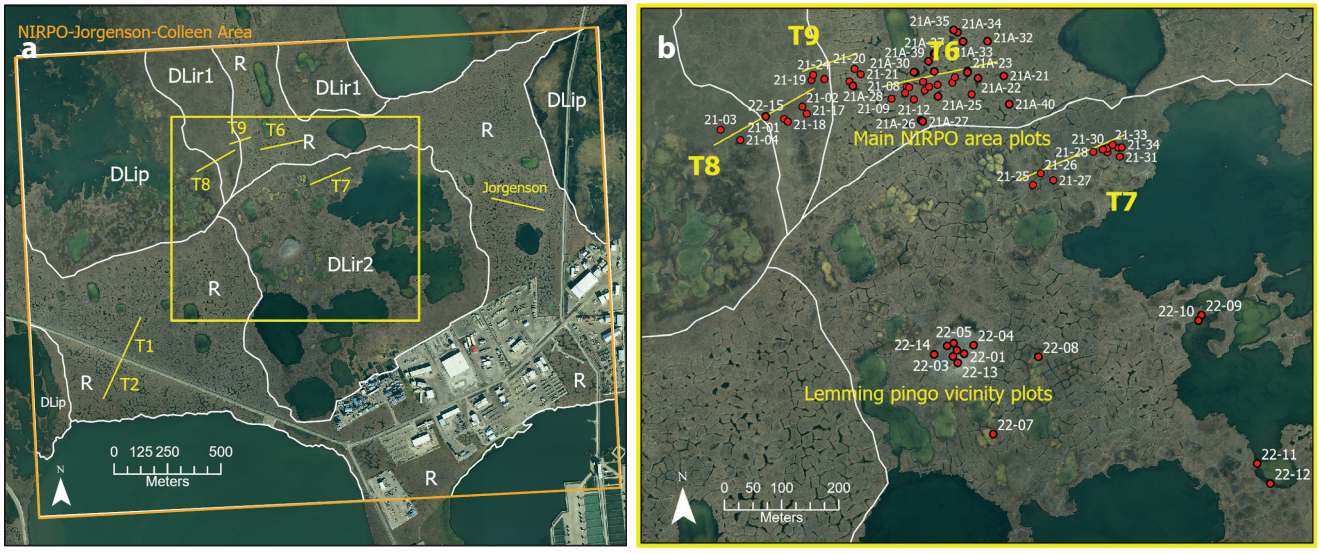

Figure 2. *The NIRPO Study Area.* ***a.*** *The NIRPO site (yellow rectangle) within the larger NIRPO-Jorgenson-Colleen research area. The landforms (white boundaries) are derived from surficial-geology units (Rawlinson 1993): R = residual surface; DLip = drained lake basin, ice poor; DLir1 = drained lake basin, ice rich, phase 1; DLir2 = drained lake basin, ice rich, phase 2.* ***b.*** *Locations of NIRPO vegetation plots. Credit: Martha Raynolds.*

mocky terrain, zoogenic features such as bird mounds and animal dens), as well as featureless terrain.

Surficial-feature elements are common "parts" of surface features (e.g., ice-wedge polygon basins, rims, and troughs, frost-boil centers and interboil areas, bird mounds, hummocky, and featureless areas) that more or less correspond to "microsites" of previous legends (e.g., Walker et al. 2023). The lower-case surficial-feature-element codes can be attached to the surface-feature codes for mapping purposes.

Table 1. *Abbreviated legends for characterizing plots and maps by surficial geology, landforms, surficial features, surficial-feature elements, and vegetation habitats at the NIRPO site. Legends codes are arranged alphabetically within each category, except for Vegetation Habitats, which are arranged in four groups along a site-moisture gradient.*

Surficial geology	
Codes and boundaries mapped by Rawlinson (1993) and used in Tables A1 and A2.	
Qsg	Undifferentiated Quaternary-age, alluvial sand and gravel deposits with overlying windblown silt and peat
Qt	Thaw-lake deposit
Qti	Ice-rich thaw-lake deposit
Landforms	
These codes correspond to characteristic landforms within the surficial geology units mapped by Rawlinson (1993).	
DL. Drained lakes	
DLip	Drained lake basin, ice poor
DLir	Drained lake basin, ice rich
DLir1	Drained lake basin, ice rich, Phase 1, some ice wedges, and mainly disjunct low-center polygons
DLir2	Drained lake basin, ice rich, Phase 2, well-developed ice wedges and low-center polygons
L. Lakes and ponds	
L1	Deeper lake, including undrained thaw lakes and deeper water bodies remaining after partial drainage
L2	Shallow lake or pond with marl bottom
L3	Ice-wedge thermokarst pond
P	Pingo
R	Residual surface
Surficial features	
Codes are based on units in previous legends (e.g. Everett, 1980, Walker et al. 2023.) The terminology follows Everdingen 2005 where applicable.	
AH	Aligned hummocks
BM	Bird mound
DP	Disjunct polygon rims
FB	Frost boils
H	Hummocky terrain
HCP1	High-center or flat-center ice-wedge polygon, < 0.5 m center-trough relief
HCP2	High-center or flat-center ice-wedge polygon, ≥ 0.5 m center-trough relief
IP	Irregular pattern, mixed features
L1	Deeper lake or ponds (> 1 m deep)
L2	Shallow lake with marl bottom
L3	Thermokarst pond
LCP1	Low-centered ice-wedge polygon, < 0.3 m center-trough relief
LCP2	Low-center ice-wedge polygon, ≥ 0.3 m center-trough relief
N	Non-patterned ground (featureless)
RP	Reticulate pattern (small polygons, < 2 m diameter, generally on well-drained sites)
TP1	Transitional polygon (with remnant polygon rims), < 0.5 m center-trough relief
TP2	Transitional polygon (with remnant polygon rims), ≥ 0.5 m center-trough relief
Z	Zoogenic features, including pingo summits fertilized by small mammals, animal dens, burrows, and bear diggings; bird mounds have their own unit (BM)
Surficial-feature elements	
These common "parts" of surface features more or less correspond to "microsites" of previous legends (e.g., Walker et al. 2023). The lower-case codes can be attached to the surface feature for mapping purposes.	
b	Center (basin) of low-center polygon
c	Center of flat- or high-center polygon or transitional polygon
i	Irregular topography associated with degraded troughs and/or collapsed polygon rims
n	None
r	Rim, includes rims of disjunct polygons, intact low-center polygons, and remnant rims on transitional polygons.
t	Trough of ice-wedge polygon

Continued on next page

Table 1 *(continued)*

Vegetation habitats	
The 17 habitat types occurring within the 59 NIRPO plots are starred (*). Previous codes from Walker 1985 and recent AGC data reports (Walker et al. 2022a, 2023) are in the first set of parentheses for each unit. Dominant or frequent species are enclosed in the second set.	
D. Dry nonacidic tundra. Dominant plant functional types: Prostrate evergreen shrubs, cushion forbs, crustose lichens, acrocarpous mosses	
D1*	(B1) Dry nonacidic tundra, cold, windblown, gravelly sites. *(Dryas integrifolia, Oxytropis nigrescens, Lecanora epibryon)*
D2*	(B2) Dry to moist nonacidic tundra on fine-grained, organic-rich soils. *(Dryas integrifolia, Saxifraga oppositifolia, Salix reticulata)*
D2t	(--) Transitional dry tundra on organic-rich soils; transitional dry tundra due to change in drainage, most closely resembling type D2
D3t	(B16d, B17d, U10d) Transitional dry tundra with dry riparian components *(Salix ovalifolia, S. lanata, Dryas integrifolia, Carex capillaris, Hulteniella integrifolia*)
Dfb	(B3) Dry to wet nonacidic sparsely-vegetated frost-boils *(Saxifraga oppositifolia, Juncus biglumis)*
Dsn*	(U6) Dry to moist, and nonacidic, early-melting, snowbeds *(Cassiope tetragona, Dryas integrifolia, Masonhalea richardsonii)*
Dz*	(U10) Dry nonacidic zoogenic vegetation, mostly on pingo summits and animal disturbances on south-facing slopes *(Festuca baffinensis, Cerastium beeringianum, Syntrichia ruralis)*
M. Moist nonacidic tundra. Dominant plant functional types: Graminoids (sedges), prostrate deciduous and evergreen shrubs, pleurocarpous mosses	
M1*	(U3) Moist nonacidic tundra with abundant lichens *(Eriophorum triste, Dryas integrifolia, Salix reticulata, Tomentypnum nitens, Thamnolia subuliformis)*
M2	(U2) Moist nonacidic tussock tundra *(Eriophorum vaginatum, Dryas integrifolia, Salix reticulata, Tomentypnum nitens, Thamnolia subuliformis)*
M3*	(U4) Moist nonacidic tundra with few lichens *(Eriophorum triste, Dryas integrifolia, Salix arctica, Tomentypnum nitens)*
M3d	(U3d, U4d, B10d, B16d, B17d) Disturbed tundra due to dust or other anthropogenic disturbance, most closely resembling moist nonacidic tundra (type M3)
M3t*	(--) Transitional moist nonacidic tundra; transitional tundra due to change in drainage, most closely resembling moist nonacidic tundra (type M3)
Msh	(U8) Moist nonacidic riparian low shrublands *(Salix lanata, S. alaxensis)*
Mz*	(U10) Moist zoogenic vegetation on bird mounds and moist animal disturbances *(Carex scirpoidea, Arctagrostis latifolia, Cerastium beeringianum, Sanionia uncinata)*
W. Wet nonacidic tundra. Dominant plant functional types: Graminoids (sedges), pleurocarpous mosses	
W1*	(M2) Wet nonacidic mires with saturated soils *(Carex aquatilis, Eriophorum angustifolium, Drepanocladus brevifolius)*
W1d	(M2d) Disturbed tundra due to dust or other anthropogenic disturbance, most closely resembling wet nonacidic tundra (type W1)
W2*	(M4) Very wet nonacidic mires with shallow standing water *(Carex aquatilis, Scorpidium scorpioides)*
W2t	(--) Very wet transitional nonacidic mires; transitional tundra due to change in drainage, most closely resembling wet nonacidic tundra (type W2)
Wz	(--) Wet zoogenic and enriched tundra; rich wet nonacidic tundra due to anthropogenic or zoogenic enrichment
A. Aquatic minerotrophic vegetation. Dominant plant functional types: Graminoids (sedges and grasses), aquatic forbs, pleurocarpous mosses	
A1*	(E1) Aquatic sedge marsh *(Carex aquatilis, Eriophorum angustifolium)*
A1t*	(M4/E1, E1t) Transitional aquatic vegetation dominated by sedges *(Carex aquatilis, Scorpidium scorpiodes)*
A2*	(E2) Aquatic grass marsh *(Arctophila fulva)*
A3t*	(E3, Em) Aquatic moss marsh *(Scorpidium scorpioides; Calliergon richardsonii)*
A4t*	(Ef) Aquatic forb marsh *(Hippuris vulgaris; Ranunculus gmelinii; Sparganium hyperboreum)*
L	Unvegetated water in lakes and ponds
L1	(W1) Lakes with deeper water generally >1 m deep (dark colored lakes on aerial images)
L2*	(--) Shallow ponds and lakes with marl bottoms (light colored lakes, ponds (includes barren intermittent marl pond margins on aerial images)
L3*	(--, Es) Thermokarst ponds with sparse undifferentiated vegetation (used mainly for mapping ponds, where aquatic vegetation is difficult to determine)

Twenty-eight vegetation habitats are listed in Table 1. These are grouped according to the five broad habitat categories (D, Dry nonacidic tundra; M, Moist nonacidic tundra; W, Wet nonacidic tundra; A, Aquatic vegetation; and L, generally unvegetated or sparsely vegetated lakes or ponds. The names of the units within each habitat category are derived from vegetation units described earlier (Walker 1985, Walker et al. 2015, 2016, 2022a, 2023, Watson-Cook 2022) and are meant to be compatible with international habitat types (Davies et al. 2004, Mucina et al. 2016, Walker et al. 2018b).

2.1.2 Aboveground biomass methods

Biomass sampling and sorting procedures described in Walker et al. 2023 (p. 8) are summarized here:

Terrestrial biomass. A 50-cm x 20-cm (0.1 m^2) aluminum sampling frame was nailed to the tundra near each plot in an area that matched as closely as possible the composition and structure of the vegetation in the plot. The tundra within the frame was cut around the inner margin of the frame with a bread knife. An additional cut was made to divide the sample in half, forming two 25-cm x 20-cm subsamples. The frame was then removed, and each half was cut horizontally 2–3 cm beneath the tundra surface. Each half sample was removed from the sample area and placed in a 1-quart Ziploc® bag with the plot number, date of harvest, and the sample half (e.g., 1 of 2 or 2 of 2) recorded on the bag and on a Post-it® note placed inside the bag.

The samples were frozen for transport to UAF, where they were kept frozen until removed for processing and thawed. The aboveground plant parts were clipped with scissors and sorted into plant functional types (PFTs): evergreen shrubs, deciduous shrubs (leaves and woody stems), graminoids (live

and dead), horsetails, forbs, mosses, lichens, and litter. Mass values for each PFT in each 0.1-m^2 sample plots were multiplied by 10 to obtain biomass per 1-m^2. Important considerations were: (1) The sorted moss component included both the green surface layer and the dead component to the level where the moss lost its structure and became part of the top organic soil layer. (2) Windblown silt is common in the study area and is known to influence the determination of organic-matter content. Many soil horizons that appear to be organic horizons have too much windblown silt to be classified as organic horizons according to the U.S. Soil Survey criteria (Everett and Parkinson 1977). (3) The moss component was washed to remove as much windblown silt as possible, but it is likely that many of the moss samples still contained an unknown amount of mineral material, and the reported moss mass values are probably high.

Aquatic biomass. A coring device was developed for sampling biomass and soils in thermokarst ponds (Watson-Cook 2022). The cylindrical cores had a diameter (D) of 15.24 cm (6 in) (cross-section area of approximately $\pi r^2 = 182.42$ cm^2). The sample of aboveground biomass was removed by slicing the core with a knife at the sediment surface. The biomass samples were then thoroughly washed in the field to remove trapped mineral sediment before freezing. Upon thawing in the lab, the core was again washed and then sorted by plant growth forms and dried according to the same procedures as the terrestrial vegetation plots. To obtain biomass per 1 m^2, the biomass values for the sample area of the aquatic plots were multiplied by 54.82 (number of sample areas per m^2).

All biomass samples were dried at 65 °C until a constant mass was obtained (approximately one week). PFT and total biomass data for NIRPO plots are in Walker et al. 2023, Appendix 8.

2.1.3 Colleen and Airport plots

LAI and NDVI data were also collected from 46 plots in disturbed roadside areas at the Colleen site (Walker et al. 2015) and Airport site (Walker et al. 2016, 2018a) (Figure 3). The data from these plots are included in this report, but they are not analyzed with the NIRPO plots because of the lack of biomass data from these sites and other differences in the baseline datasets.

The Colleen site was described in publications that focus on the impact of the Spine Road on vegetation, hydrology, and permafrost within 200 m of the road (Kanevskiy et al. 2017, 2022, Walker et al. 2022a). Transects T1 and T2 are in an area of transitional ice-wedge-polygons that have extensive thermokarst ponds. The primary impacts are caused by heavy road dust on the northeast side of the road. Road dust plus extensive roadside flooding occurs on the southwest side of the road. The Colleen plots are located in paired ice-wedge-polygon centers and troughs at 5, 10, 25, 50, 100, and 200 m from the road (24 plots total).

Plots along Airport transects T3 and T4 are distributed in polygon centers and troughs along 100 m transects on both sides of the road (20 plots total). Disturbances at the Airport site are more varied and more severe than at the Colleen site and include impacts from the 2015 Sagavanirktok flood (Shur et al. 2016, Toniolo et al. 2017, Kaneveskiy et al. 2022, Walker et. al. 2016, 2018a, Zwieback, 2023). Airport transect T5

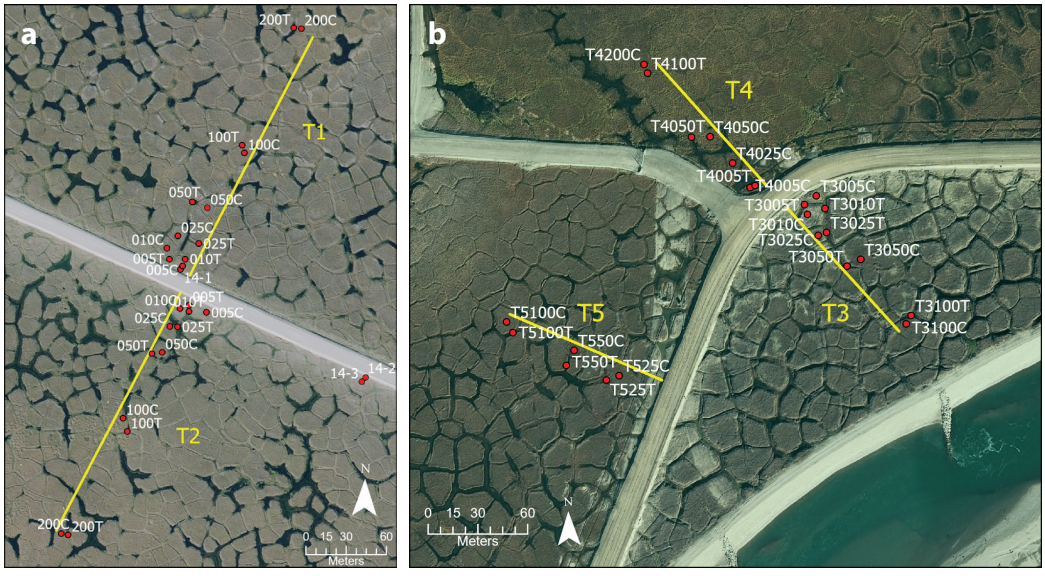

Figure 3. *Locations of plots in disturbed tundra along five roadside transects at the* ***a.*** *Colleen and* ***b.*** *the Airport sites. Credit: Martha Raynolds.*

begins at 25 m from the road (to avoid an area heavily disturbed by fiber-optic cable trenches) and extends to 100 m (6 plots total).

2.2 Grouping plots into moisture categories

2.2.1 Earlier concepts of site-moisture gradients in the Prudhoe Bay region

The NIRPO conceptual site-moisture gradient builds on ecological investigations in the Prudhoe Bay region conducted in the 1970s by the International Biological Program's Tundra Biome that recognized the key roles of soil pH, site moisture, and the permafrost table for defining soil and vegetation units along meso- and microtopographic gradients (Webber and Walker 1975; Everett and Parkinson 1977, Walker et al. 1980, Walker 1985, Walker and Everett 1991).

A conceptual meso-topographic catena for a portion of the Prudhoe Bay region portrays vegetation types and soils of the region along a small slope with approximately 2–3 m of vertical relief (Figure 4a, Walker 1985). Dry plant communities and soils occur on the top and shoulder of the slope; moist vegetation and soils occur on backslope and footslope; wet vegetation in the flatter toe slope and plain at the bottom of the slope; and aquatic vegetation in the margin of a small lake.

Figure 4b depicts the effects of microtopographic relief on soils and vegetation in a series of six ice-wedge polygons, from dry high-center polygons with over 0.5 m of relief near a small stream to very wet low-center polygons with shallow late-summer water in the polygon basins, and less than 0.3 m of topographic relief (Walker 1985). This depiction applies to the eastern nonacidic portion of the oilfield in the 1970s and 1980s, before extensive ice-wedge melting and trough subsidence began, and when most low-center ice-wedge polygons had troughs that were approximately at the same elevation as the polygon centers, without standing water. Many current ice-wedge polygons, soils, and vegetation are in transitional states related to changes in drainage status associated with the degradation of ice wedges and increase in thermokarst ponds (Jorgenson et al. 2006, 2022, Raynolds et al. 2014, Kanevskiy et al. 2017, 2022, Frost et al. 2022).

A major factor affecting soil moisture measurements is the amount of windblown silt. Most of the Prudhoe Bay region spans areas influenced by calcareous loess blown from the broad alluvial floodplain of

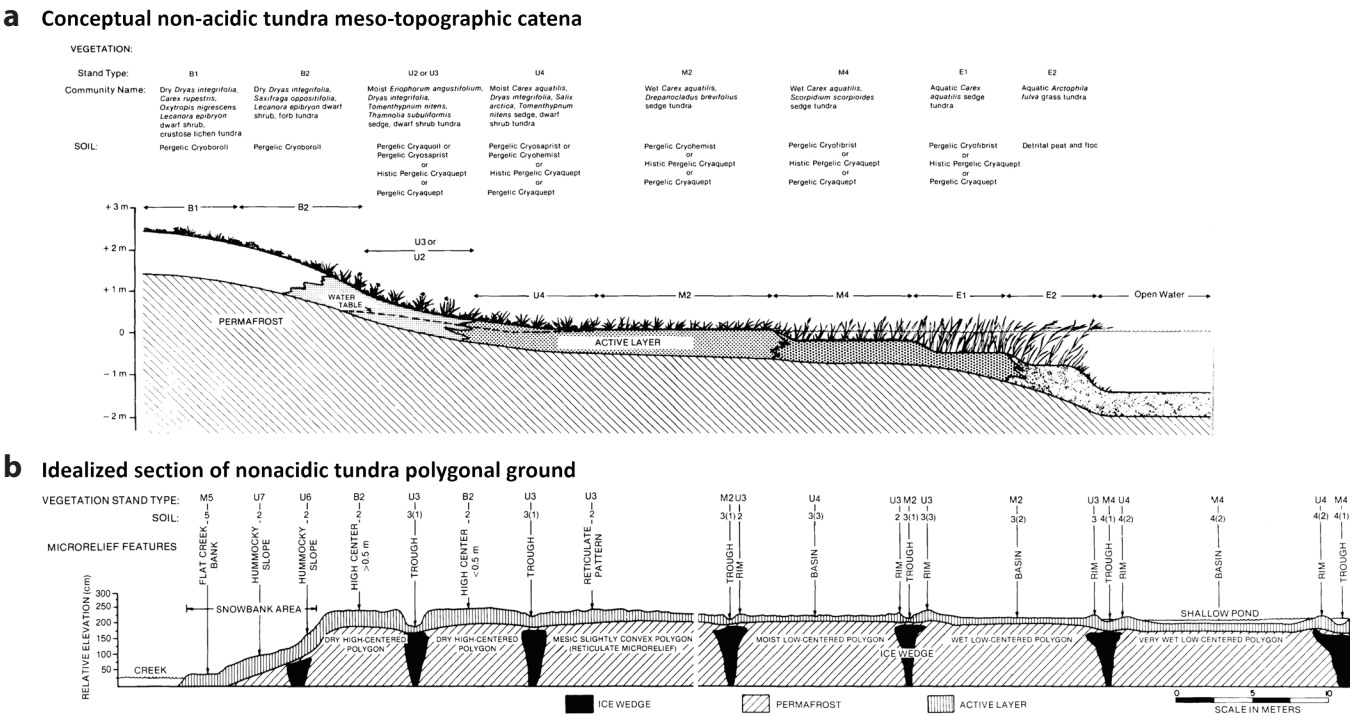

Figure 4. *Conceptual sections of terrain and soil variation along the site-moisture gradient, Prudhoe Bay region, Alaska.* ***a.*** *Mesotopographic moisture catena with typical soils and vegetation (Walker 1985). The soil types were classified by Everett and Parkinson (1977).* ***b.*** *Idealized section of tundra showing various types of ice-wedge polygons (Walker 1985). Codes refer to typical vegetation and soil mapping units described in the Geobotanical Atlas of the Prudhoe Bay Region, Alaska (Walker et al. 1980) and are cross referenced in Table 1. Note reference to permafrost and active layer in both figures.*

the Sagavanirktok River (Everett and Parkinson 1977, Walker and Everett 1991). The addition of mineral material to the organic soil surface horizons increases soil bulk density and decreases its water-holding capacity.

2.2.2 Data used to define the conceptual site-moisture gradient

The conceptual site-moisture gradient used in this report is specific to the nonacidic tundra at the NIRPO site and includes vegetation habitat types described for the study site in recent publications, including dry and transitional-tundra types, zoogenic plant communities, and aquatic lake vegetation types. Subjective field estimates of site and soil moisture along with laboratory measurements of gravimetric and volumetric soil moisture were used to help define the conceptual site-moisture gradient.

Field estimates of site moisture and soil moisture. Subjective (scalar) estimates of site moisture at the ground surface (Table 2a) and soil moisture in the rooting zone (Table 2b) were made during the NIRPO vegetation surveys in 2021 and 2022 (Walker et al. 2022a, 2023).

Laboratory measures of soil moisture. Soil plugs 15 x 15 cm in area and 40 cm long were collected using a tile spade from sites immediately adjacent to each 1 x 1 m plot. The major soil horizons were briefly described. A soil sample was removed from the top of the mineral horizon just below the organic soil horizons using a 180 cm^3 soil can. Soil analyses were conducted at the UAF Forest Soils Lab. Gravimetric soil moisture was calculated by weighing the wet sample, oven drying it at 105 °C for 24–48 h, reweighing, and calculating the mass of water lost as a percentage of the mass of the dried soil. Volumetric soil moisture was calculated as the volume of water lost during drying as a percentage of the volume of the soil can (180 cm^3). Other soil data from the samples, including wet and dry color, bulk density, particle analysis, total organic matter, and soil pH are reported in earlier NIRPO data reports (Walker et al. 2022a, 2023).

2.2.3 Arrangement of the NIRPO vegetation habitat types along the conceptual site-moisture gradient

The 59 NIRPO plots were grouped according to four broad site-moisture categories (Dry tundra, Moist tundra, Wet tundra, Aquatic vegetation). Eight of the plots, all on Lemming Pingo, were considered "Dry tundra" (site-moisture codes 3 and 4, xeric to subxeric); 18 plots were considered "Moist tundra" (codes 5 and 6, mesic); 13 were "Wet tundra" (codes 7 and 8, subhygric), 15 were "Aquatic," and 5 were "Lake" or ponds with sparse or no vegetation (hygric and hydric, codes

Table 2. *Site and soil moisture scales used in the NIRPO plot vegetation surveys (modified from Komárková 1983).*

a. Site moisture scale	
Code	**Description**
1	**Extremely xeric**, almost no soil moisture, no plant growth, e.g., extreme polar desert
2	**Very xeric**, very little soil moisture, e.g., dry sand dunes
3	**Xeric**, little soil moisture, e.g. stabilized sand dunes, dry ridge tops
4	**Subxeric**, noticeable soil moisture, e.g., well-drained slope, ridges
5	**Subxeric to mesic**, slightly moist site, e.g., upper slopes of gently sloping terrain
6	**Mesic**, moderate moisture, e.g., many zonal sites on gentle slopes or raised microsites
7	**Mesic to subhydric**, considerable late-season moisture, saturated soils, depression but usually without late-season standing water, e.g., lower slopes, depressions with saturated soils
8	**Subhydric**, considerable moisture, saturated soils throughout summer, with occasional standing water, less than 10 cm deep
9	**Hydric**, aquatic sites with up to 100% of the surface with standing water 10–50 cm deep most of the summer
10	**Hydric**, aquatic sites with deeper water 50–150 cm deep
b. Soil moisture scale	
Code	**Description**
1	**Very dry**, very little moisture, soil does not stick together
2	**Dry**, little moisture, soil somewhat sticks together
3	**Damp**, noticeable moisture, soil sticks together but crumbles
4	**Damp to moist**, very noticeable moisture, soil clumps
5	**Moist**, moderate moisture, soil binds but can be broken apart
6	**Moist to wet**, considerable moisture, soil binds and sticks to fingers
7	**Wet**, considerable moisture, water drops can be squeezed from the soil
8	**Very wet**, much water can be squeezed from the soil
9	**Saturated**, water drips from the soil
10	**Very saturated**, soil is more liquid than solid

9 and 10). The A and L vegetation habitat codes were used for mapping to separate deeper lakes and ponds with little or no vegetation from aquatic sites with considerable vegetation.

Finer-level habitat characterizations within the broad site-moisture categories were based on habitat types described in earlier data reports (e.g., Walker et al. 2022a). Representative photos of 16 of vegetation habitats are in Figure 5. Plot data regarding plant-community composition, growth-form structure, biomass, soils, site factors, and photos were obtained from previous data reports for the NIRPO, Colleen, and Airport sites (Walker et al. 2022a, 2023).

Site moisture (scalar) and volumetric soil moisture were used to help align the vegetation habitats along the conceptual site-moisture gradient. Figure 6a shows the distribution of site-moisture scores grouped by the four broad site moisture categories. Variation in site moisture for the 17 vegetation habitats within these four categories are displayed in Figure 6b. Scalar values of site moisture are visually interpreted in the field based on the amount and depth of surface water and saturation of the soil surface. The subjective measurements provided a clear separation for the four moisture groups and a generally clear trend for the 17 vegetation habitats, although there were areas of score overlap between some habitats.

There was less clear separation of volumetric soil moisture values of the four site-moisture groups and the 17 vegetation habitat types (Figure 6c and d) than with scalar estimates of site moisture (Figure 6a and b). Variation in volumetric soil moisture can be caused by numerous factors related to, for example, variation in the degree of soil organic matter and soil texture within soil profiles and also to inconsistent methods of collecting the soil samples.

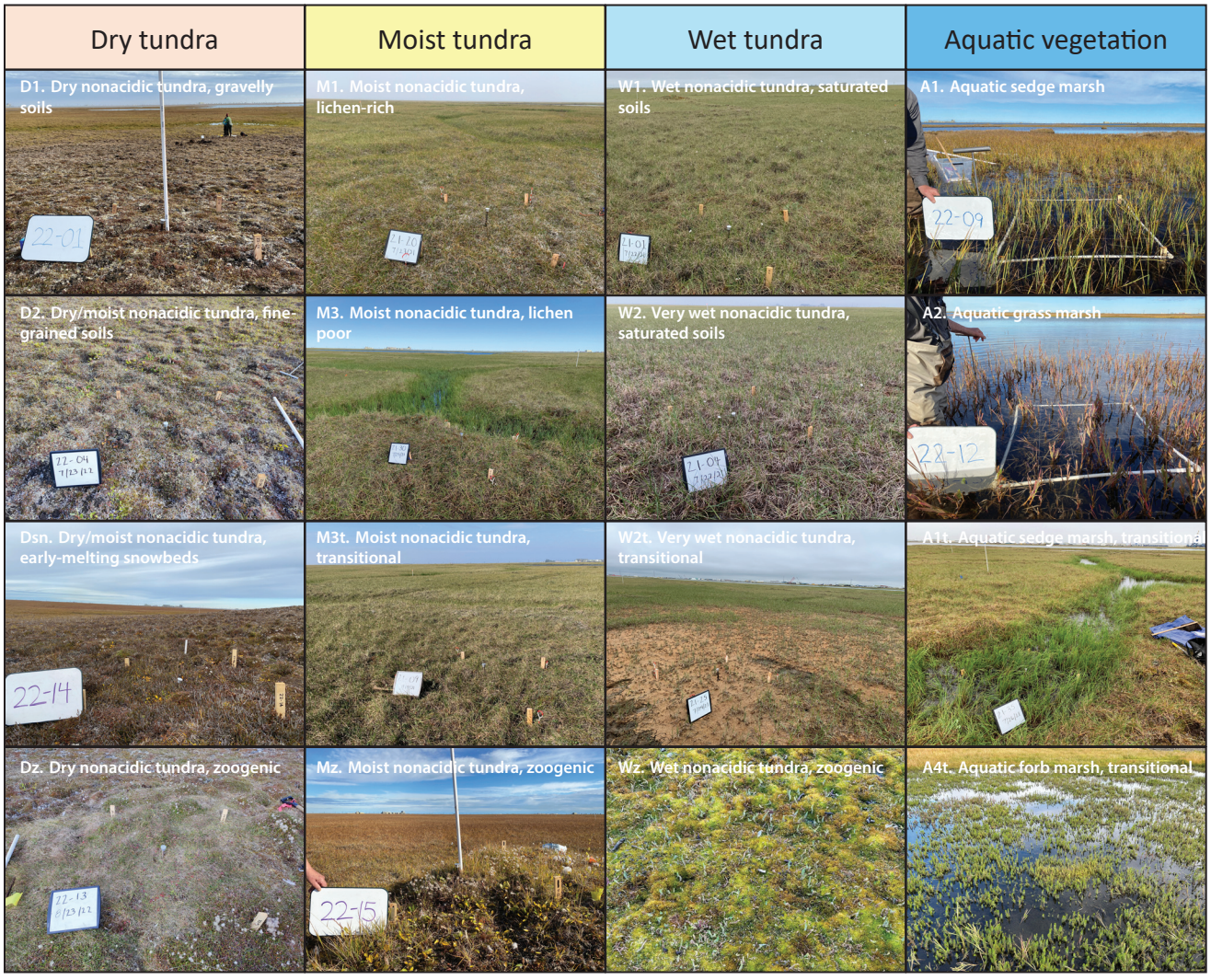

Figure 5. *Examples of major vegetation habitats within the four broad site-moisture groups. Credit: Wz and A4t by Olivia Hobgood. All other photos by Amy Breen.*

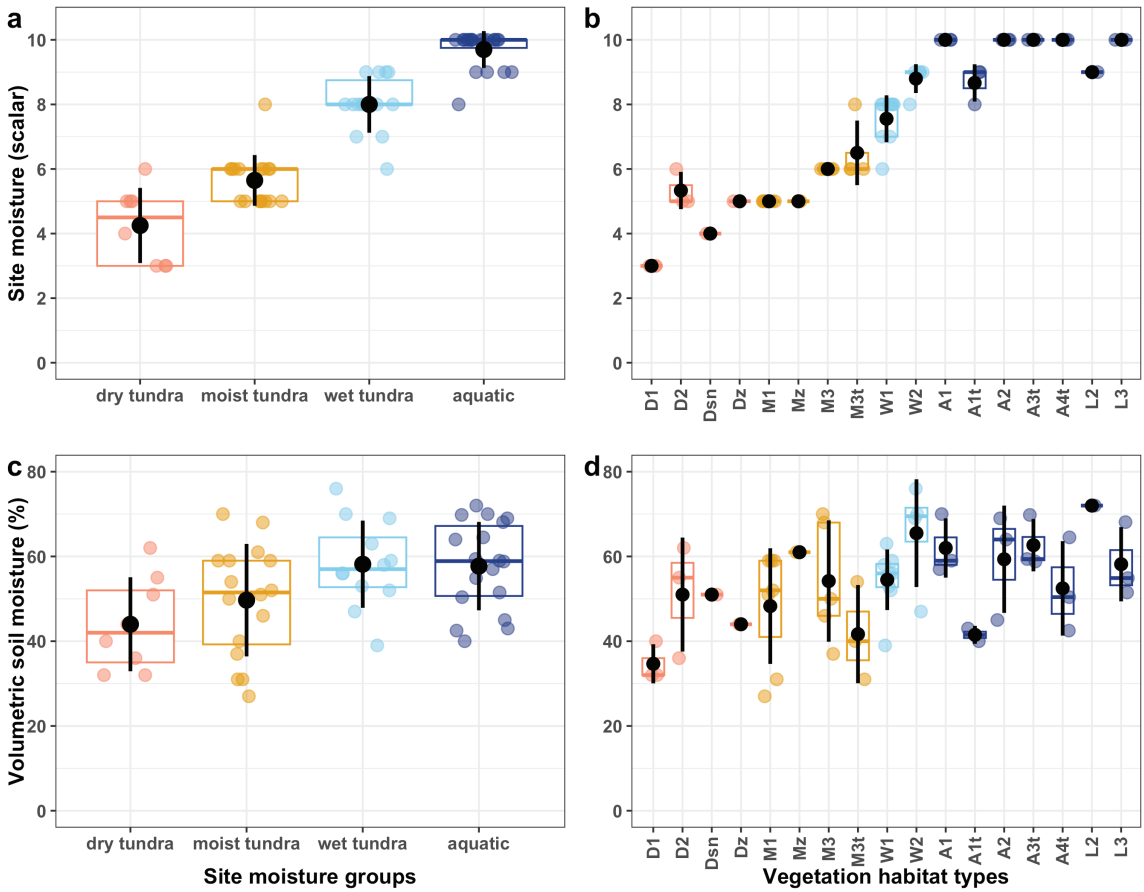

Figure 6. *Distribution of scalar site-moisture scores and volumetric soil-moisture values across the conceptual site-moisture gradient.* ***a.*** *Scalar site-moisture scores by four broad site-moisture groups.* ***b.*** *Scalar site-moisture scores by 17 vegetation habitat types.* ***c.*** *Volumetric soil moisture by four broad site-moisture groups.* ***d.*** *Volumetric soil moisture by 17 vegetation habitat types. The box-plot diagrams show the mean value (black dots), standard deviation (error bars), median (middle value in the data set, colored horizontal line within the boxes), first quartile (median value of the lower half of the dataset, lower limit of the boxes), and third quartile (median value of the of upper half of the dataset, upper limit of the boxes.*

2.3 LAI measurements

Nondestructive measurements of LAI were made using a LI-COR LAI-2000 Plant Canopy Analyzer (Figure 7a). The instrument contains a fish-eye optical sensor (148˚ field of view) that measures radiation in a nearly hemispheric view of the sky. The method includes an above-canopy measurement of diffuse sky radiation, which was compared with the mean of four below-canopy measurements to determine how much of the above-canopy radiation is attenuated by the vegetation canopy (Figure 7b). The instrument calculates the light transmittance for each below-canopy measurement based on the above-canopy value.

The center plot markers were removed to avoid interference with the measurements. The readings were all taken with a 270˚ view cap over the lens to exclude view of the observer from the sensor. The measurements were taken with the sensor placed in the shadow of the observer during each measurement to reduce varying light conditions in the plant canopy (Figure 7c). One above canopy measurement was taken from the center of the plot with the instrument held level, followed by four below-canopy measurements taken at the ground surface near the center of each of the four quarters of the plot. After the fourth below-canopy measurement, the control-unit displayed six values: (1) mean LAI; (2) standard error of the LAI (SEL); (3) diffuse non-interceptance (DIFN), which is the fraction of sky visible to the sensor; (4) mean tilt angle of the sensor (MTA); (5) standard error of the MTA (SEM); and (6) the number of pairs of above- and below-canopy observation included in the calculations (SMP). In some cases, one or more of the below-canopy readings were rejected for various reasons including: (1) rapid changes in the light conditions, (2) a non-level instrument, or (3) very little erect vegetation or extensive water cover. In these cases,

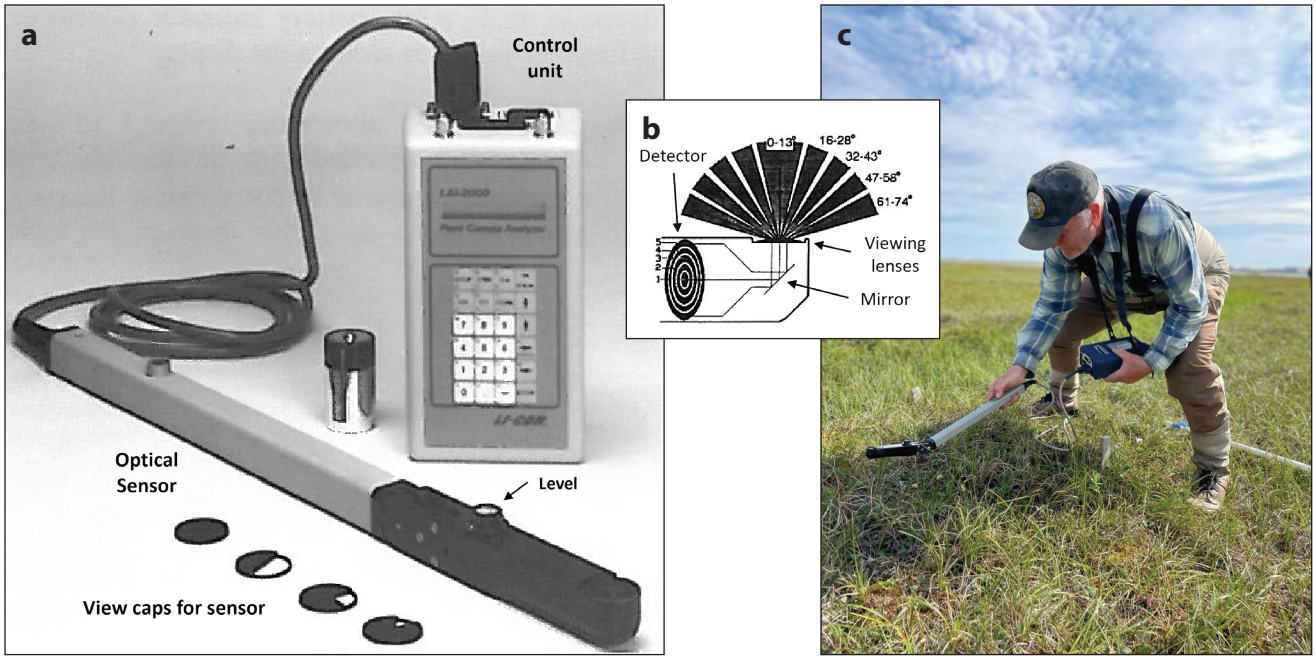

Figure 7. *LI-COR LAI-2000 Plant Canopy Analyzer.* ***a.*** *The LAI 2000, includes the control unit, optical sensor with handle, level, fish-eye lens at the end of the sensor, and view caps for excluding part of the sky.* ***b.*** *Schematic of the fish-eye lens end of the sensor. The light is reflected off a mirror to detectors arranged in five concentric rings from zenith (0˚) to 74˚. Photo and image, LI-COR, Inc.* ***c.*** *Above-canopy measurement under partly cloudy conditions, with the sensor in the shadow of the observer with 270˚ view cap over the lens to exclude view of the observer. (Note the position of the fish-eye canopy viewing lens, which is approximately 2 cm above the ground surface when the sensor is placed flat on the ground.) Credits: a and b, LI-COR Inc.; c, Amy Breen.*

new measurements were made until at least three measurements were included in the calculations. The theory and mathematics for calculating the LAI from the measurements are in the LAI-2000 Operating Manual (LI-COR, Inc. 1992).

2.4 NDVI measurements

NDVI is an index of photosynthetic capacity or chlorophyll content (greenness of vegetation), which is calculated from the reflectance of the vegetation in the near-infrared (NIR) and red (R) bands of the spectrum using the formula: NDVI = (NIR – R)/(NIR + R). Vegetation absorbs red light for photosynthesis and reflects near-infrared light. The difference in the reflectance of the NIR and R bands varies between 0 and 1. Bare soil generally has NDVI values close to zero; sparse vegetation generally has low NDVI values (0–0.05), and dense chlorophyll-rich vegetation generally has high values (>0.6); and plots with large components of open water often have negative NDVI values.

NDVI measurements were taken with a Spectra Vista Corporation (SVC) i-Series field-portable spectroradiometer (model HR-1024i) (Figure 8a) using a 25° fiber-optic light guide with the spectrometer carried in a backpack (Figure 8b). The measurements were made at each plot immediately preceding the LAI measurements. A standard reflective whiteboard with near 100 percent reflectivity was used for solar radiation reference readings, followed by a target reading in each of the four quadrants of each 1 m^2 plot (totaling one reference reading and four target NDVI readings per plot). The reference whiteboard was attached to a leveled tripod roughly 1 m off the ground (Figure 8c). All spectral-reflectance measurements were also taken at about 1 m above the ground, in consistent light conditions, avoiding shadows and interference from plot markers or the observer. Near-infrared reflectance NIR (858 nm wavelength) and red (648 nm) reflectance were used to calculate NDVI. The four target measurements were averaged to attain average NDVI per plot.

Other data collected at the time of the LAI and NDVI measurements included: (1) height of the plant canopy (four measurements in the centers of the 4 quarters of the plot) (2) an estimate of the percentage of the plot covered by water, and (3) a photo of the plot. Snow depths were measured on all the plots 30 April–May 3, 2024.

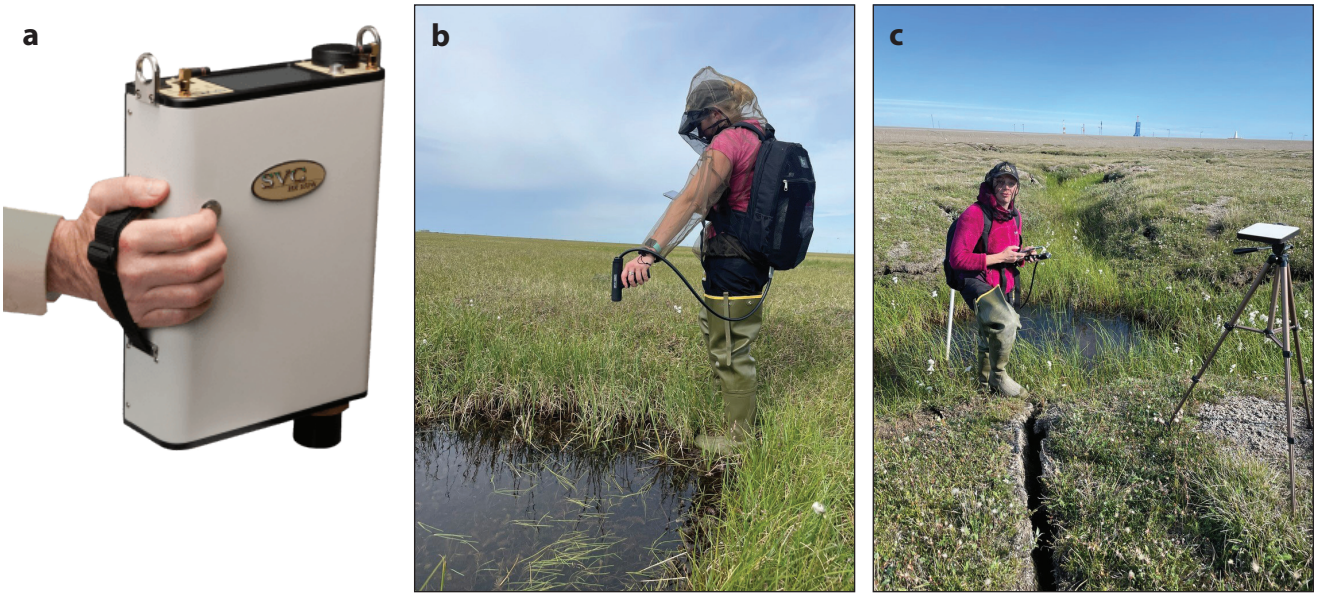

Figure 8. ***a.*** *Spectra Vista Corporation (SVC) field-portable spectroradiometer, model HR-1024i.* ***b and c.*** *Kelcy Kent making field measurement of NDVI with the spectrometer carried in a backpack linked and a fiber-optic cable to a hand-held 25˚ field of view radiation sensor. Note in* ***c*** *the reflective calibration whiteboard mounted nearby on a tripod. Credits: a, Courtesy of Spectra Vision Corp.; b and c, Amy Breen.*

2.5 Data analysis

The 59 NIRPO plots include 50 terrestrial plots (21-1 to 21-35 and 22-1 to 22-15) (Walker et al. 2023) and nine selected aquatic plots (21A-22, 26, 27, 28, 29, 35, 36, 38, 40) (from Watson-Cook 2022). These are grouped hierarchically according to four broad site-moisture categories (dry tundra, moist tundra, wet tundra, aquatic vegetation) and then into 17 vegetation habitat subunits that occur within the 59 sampled plots (Table 1).

To identify relationships between NDVI and dependent variables (LAI and aboveground biomass components), we regressed each variable separately against NDVI.

To better understand the relationship between NDVI and LAI, we also regressed these variables by site moisture type and surficial feature. To examine the relationship between plot moisture and dependent variables (NDVI, LAI, biomass components), we regressed each variable separately as well against volumetric soil moisture and our scalar soil moisture variable. Univariate regressions were conducted in Microsoft Excel with best-fit equations and R^2 presented.

To examine trends across the moisture gradient, we averaged values by habitat type for canopy height, water depth, thaw depth, snow depth, biomass components, LAI and NDVI. We present these data as bar graphs ordered from dry to aquatic.

3 Results and Discussion

Key plot data from the 59 NIRPO plots included surficial geology, landform, surficial feature, surficial-feature element, vegetation habitat, NDVI, LAI, total biomass, vegetation height, and water depth, and plot photos numbers are in Appendix Table A1. The table is arranged and colored by the four site-moisture groups (dry tundra–pink; moist tundra–yellow; wet tundra–light blue; aquatic vegetation–dark blue). Additional plot data including biomass by plant functional types, estimates of PFT cover, other site factors, and photos of all vegetation plots are in previous AGC data reports (Walker et al. 2022a, 2023).

3.1 Trends of key site variables along the site-moisture gradient

3.1.1 Vegetation height, thaw depth, water depth, and snow depth

The mean vegetation canopy height, thaw depth, water depth, and snow depth are summarized for each vegetation habitat type along the conceptual site-moisture gradient (Figure 9).

Average vegetation height increased in habitats along the soil moisture gradient from dry D1 to aquatic A1 and then declined in the deeper aquatic types

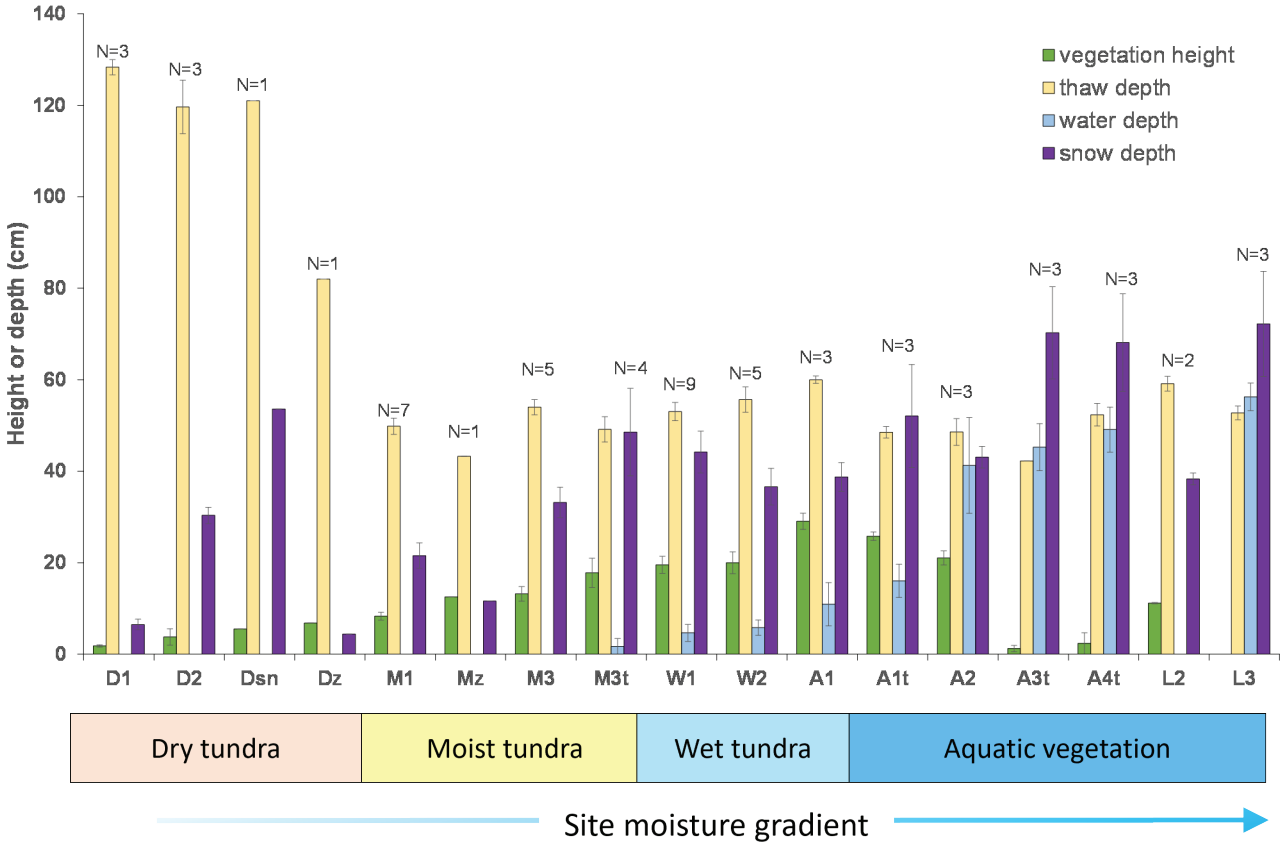

Figure 9. *Mean site characteristics (vegetation canopy height, thaw depth, water depth, and snow depth) for vegetation habitats along the NIRPO conceptual site moisture gradient. Vegetation height, thaw depth, and water depth were measured in August 2023, snow depth April 30–May 3, 2024 (Walker et al. 2022a, 2023). N values are numbers of plots. Error bars show standard deviation. Legends for the vegetation habitats are in Table 1.*

(A1t–L3). The shortest vegetation was in aquatic habitats with little emergent vegetation (A3t, A4t, L3: 0–2 cm above the water level) and the dry habitats (D1–Dsn: 2–7 cm, N = 3). The tallest vegetation was in the aquatic habitats with graminoid vegetation (A1–A2: 21–29 cm above the water level, N = 3). Intermediate heights were encountered in the moist and wet habitats (M1– L2) (20–28 cm, N = 7).

Average thaw depths were deepest in dry types D1–Dsn (120–128 cm, N = 3). The dry zoogenic community on the pingo summit (Dz) had shallower mean thaw (82 cm, N = 1), probably due to a somewhat thicker vegetative layer and a thick insulative organic-rich A horizon. Mean thaw depth varied narrowly in all other habitat types (M1–L3, 42–60 cm, N = 13 habitat types).

No standing water occurred in the dry and moist habitat types and intermittent marl pond margins (D1–M3, L2, N = 8). The moist transitional type M3t had an average of 2 cm of water. Wet types had shallow water (W1–W2, A3t: 4-6 cm, N = 3) aquatic sedge types had intermediate water depth (A1 and A1t: 11–16 cm, N = 2); and lake and thermokarst pond habitats had the deepest water (A2, A3t, A4t, and L3: 41–72 cm, N = 4).

Mean snow depths were shallowest in dry windblown habitats (D1, Dz, Mz: 4–11 cm, N = 3). The deepest snow occurred in ice-wedge thermokarst ponds and deeper troughs (A3t, A4t, L3: 68–72 cm, N = 3). The dry snowbed plot had intermediate snow depth (Dsn: 54 cm, N = 1). Dry, moist, wet, and aquatic habitats in flatter terrain had intermediate snow depths (D2, M1, M3, M3t, W1, W2 , L2, A1, A1t, A2: 22–52 cm, N = 9).

3.1.2 Biomass

Estimates of mean aboveground biomass sorted by plant-functional types are displayed for each vegetation habitat along the conceptual site-moisture gradient (Figure 10). The mean total aboveground biomass (MTAB) of the dry nonacidic tundra plots was 888 ± 271 g m^{-2} (N = 8) and ranged between 825 g m^{-2} on

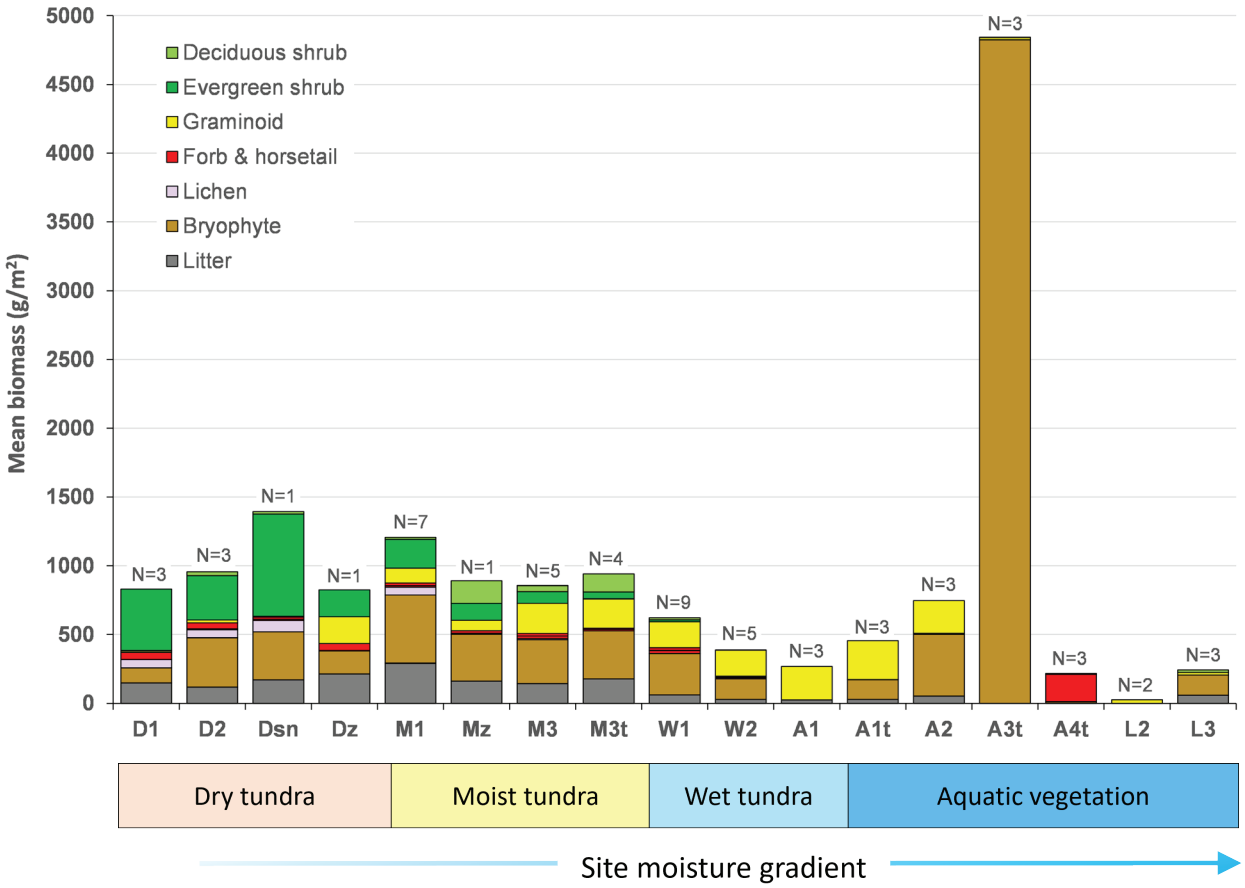

Figure 10. *Mean total aboveground biomass x plant-functional types within vegetation habitats along the NIRPO conceptual site moisture gradient. Data are from Walker et al. (2023). Legends for the vegetation habitats are in Table 1.*

the dry pingo summit (type Dz) to 1394 g m^{-2} in the dry snowbed (Dsn). The unexpected relatively high amount of biomass in dry plots was comparable to that of the moist tundra plots, due mostly to the number of woody stems of prostrate to hemi-prostrate evergreen shrubs [196 g m^{-2} on the pingo summit (Dz) to 743 g m^{-2} in the snowbed (Dz)]. *Dryas integrifolia* was the dominant evergreen shrub in all dry types, and *Cassiope tetragona* was co-dominant in the snowbed.

The MTAB in the moist nonacidic tundra plots was 1011 ± 289 g m^{-2} (N = 17) and ranged from 1198 ± 254 g m^{-2} (N = 7) in moist lichen-rich tundra (M1) to 839 ± 232 g m^{-2} m (N = 5) in moist nonacidic tundra that lacks high cover of lichens (M3). The MTAB in the wet nonacidic tundra types was 522 ± 245 g m^{-2} (N = 14) and varied between 602 ± 245 g m^{-2} (N = 9) in wet nonacidic tundra (W1) to 379 ± 219 g m^{-2} (N = 5) in very wet nonacidic tundra.

The MTAB for all aquatic vegetation was highly variable (1081 ± 1717 g m^{-2}, N = 20). Most of the variation was concentrated in the transitional types found in ice wedge thermokarst ponds and troughs, (A1t, A3t, and A4t, biomass = 1818 ± 2334 g m^{-2}, N = 9). The aquatic moss type A3t, dominated by *Calliergon richardsonii* or *Scorpidium scorpioides* had by far the greatest amount of biomass (4843 ± 1174 g m^{-2}, N = 3). Biomass was much lower and less variable, in the group of non-transitional types found in shallow marl lake margins (including types, A1, A2, L2, and L3, biomass = 347 ± 381 g m^{-2}, N = 11)

The biomass of individual plant functional types had peaks in different parts of the site-moisture gradient (Figure 11). Deciduous shrubs peaked in moist tundra; evergreen shrubs peaked in dry to moist tundra; graminoids in aquatic to moist tundra; forbs in dry tundra and aquatic forb vegetation; horsetails in wet to moist tundra; lichens in dry and moist tundra with lichens, and bryophytes in aquatic-moss vegetation. Litter was most abundant in the graminoid moist tundra types.

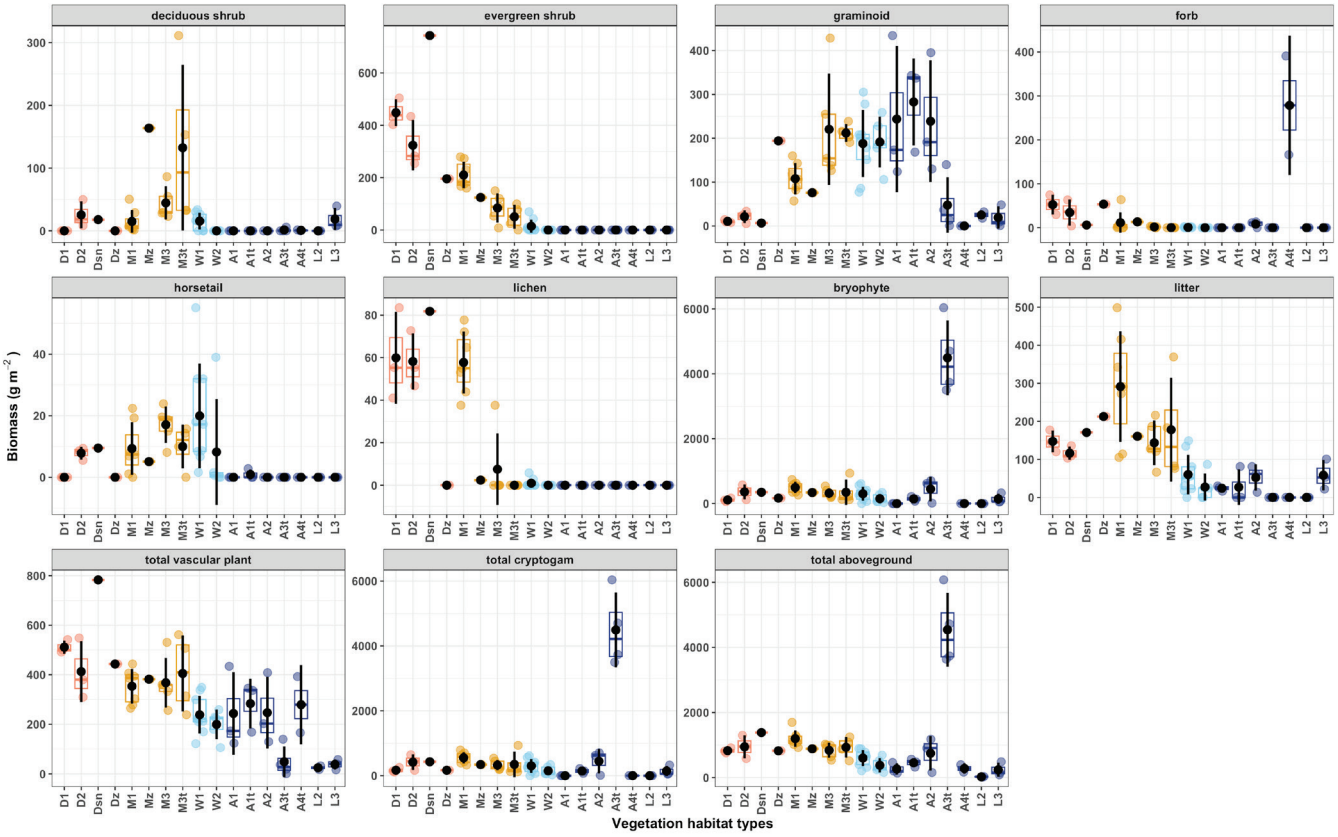

Figure 11. *Aboveground biomass of plant functional types in vegetation habitat types along the NIRPO site-moisture gradient. The box-plot diagrams show the mean value (black dots), standard deviation (error bars), median (middle value in the data set, colored horizontal line within the boxes), first quartile (median value of the lower half of the dataset, lower limit of the boxes), and third quartile (median value of the of upper half of the dataset, upper limit of the boxes). Note differences in vertical scales. Legends for the vegetation habitat are in Table 1.*

3.1.3 Trends of LAI and NDVI with site moisture

Mean LAI and NDVI are shown for the four site-moisture groups and 17 vegetation habitat types along the conceptual gradient (Figure 12). LAI and NDVI values for individual plots are in Appendix Table A1. There is a trend of generally increasing LAI from the dry habitat type D1 to the mires with saturated soils (type W1), and then there is a steep decline in both NDVI and LAI in the aquatic types where standing water affects both the LAI and NDVI values except for the transitional type A1t, which includes the subsiding thermokarst troughs with lush stands of the emergent sedge *Carex aquatilis*. Negative mean NDVI values occurred in habitats where there is deep standing water with no emergent vegetation (types A4t and L3).

The highest mean LAI values occurred in the wet group of vegetation habitats (mean LAI = 0.93 ± 0.45) (Figure 12a, b), even though this group had the lowest mean total biomass (522 ± 253 g m^{-2}). This was most likely due to relatively high proportion of taller live and standing dead sedges with vertically-oriented leaves that intercept a relatively high proportion of light despite the relatively low foliar biomass compared to lower growing prostrate shrubs with dominantly planar leaf orientation and more woody biomass that form a high proportion of the cover and biomass in the dry and moist groups of habitats.

Low mean LAI values, occurred in the dry group (mean LAI = 0.22 ± 0.32, N = 8) and the aquatic group (mean LAI = 0.29 ± 0.35, N = 20). These low values do not reflect the relatively high mean total biomass of either the aquatic group (1018 ± 1717 g m^{-2}, N = 20), where most of the biomass is below the water surface, or the dry group (942 ± 271 g m^{-2}), where much of the biomass is very low growing prostrate evergreen shrubs, mosses, and lichens. The primary component of the biomass in both of these was not sensed by the LAI-2000 viewing lens because the height of most of the vegetation did not exceed the height of the LAI radiation sensor when the instrument was placed on the soil surface (approximately 2 cm) (see Figure 8). The moist group of vegetation habitats had intermediate LAI (mean LAI = 0.53 ± 0.22, N = 17) and relatively high total biomass (1011 ± 289 g m^{-2}).

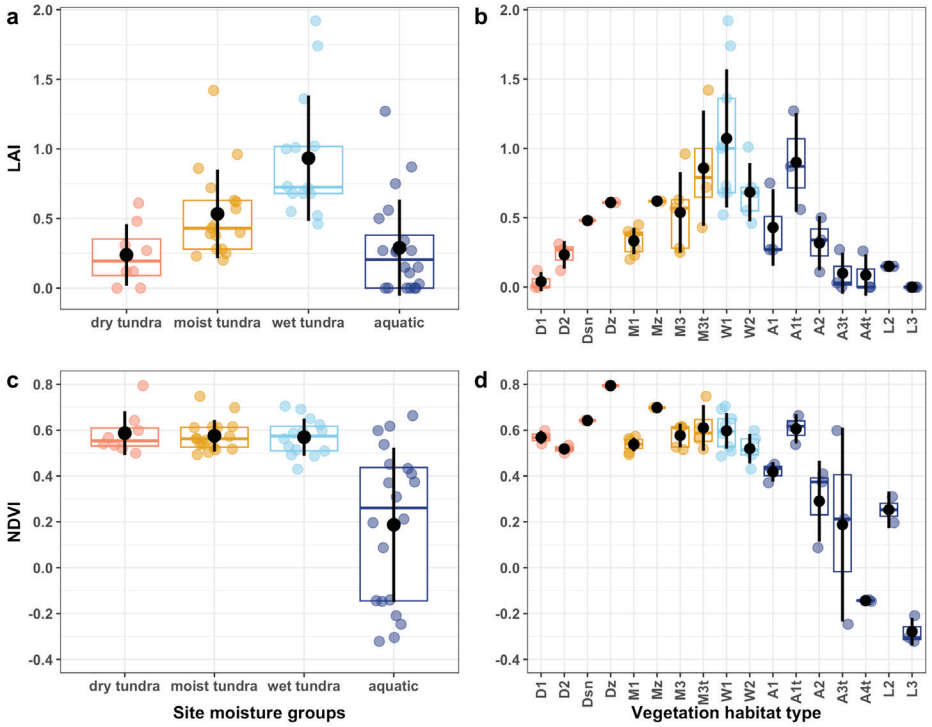

Veg habitat group	N	LAI		NDVI		Total biomass (g m^{-2})	
		Mean	SD	Mean	SD	Mean	SD
Dry	**8**	**0.22**	**0.22**	**0.59**	**0.10**	**942**	**271**
D1	3	0.04	0.07	0.57	0.03	829	80
D2	3	0.23	0.10	0.52	0.02	947	356
Dz	1	0.61		0.79		825	
Dsn	1	0.48		0.64		1384	
Moist	**17**	**0.53**	**0.32**	**0.58**	**0.07**	**1011**	**289**
M1	7	0.33	0.10	0.54	0.03	1198	254
M3	5	0.54	0.29	0.58	0.05	839	232
M3t	4	0.86	0.42	0.61	0.09	932	317
Mz	1	0.62		0.70		886	
Wet	**14**	**0.93**	**0.45**	**0.57**	**0.08**	**522**	**253**
W1	9	1.07	0.50	0.60	0.08	602	245
W2	5	0.68	0.21	0.52	0.06	379	219
Aquatic	**20**	**0.29**	**0.35**	**0.19**	**0.34**	**1018**	**1717**
A1	3	0.43	0.28	0.42	0.04	268	173
A1t	3	0.90	0.36	0.61	0.06	455	123
A2	3	0.32	0.20	0.29	0.16	748	528
A3t	3	0.10	0.15	0.19	0.42	4843	1174
A4t	3	0.09	0.15	-0.14	0.00	216	161
L2	2	0.15	0.00	0.25	0.08	25	10
L3	3	0.00	0.00	-0.28	0.06	242	214

Figure 12. *Distributions of NDVI and LAI x four site-moisture classes and 17 vegetation habitat types across the conceptual site-moisture gradient.* ***a.*** *LAI by four broad site-moisture groups;* ***b.*** *LAI by 17 vegetation habitat types;* ***c.*** *NDVI by four broad site-moisture groups;* ***d.*** *NDVI by 17 habitat types. The box-plot diagrams show the mean value (black dots), standard deviation (error bars), median (middle value in the data set, colored horizontal line within the boxes), first quartile (median value of the lower half of the dataset, lower limit of the boxes), and third quartile (median value of the of upper half of the dataset, upper limit of the boxes). Mean and standard deviation of the LAI, NDVI and biomass values are displayed in the right-hand table.*

Relatively high mean NDVI values above 0.5 occurred in dry, moist, and wet site-moisture groups (Figure 12c, d). The lowest NDVI values were in the aquatic plots, with several values below 0 in sites where most of the biomass is below the water surface.

The contrast between LAI and NDVI is largely a function of what the sensors on the two field instruments see. The LAI-2000 is an upward-viewing instrument that measures intercepted light penetrating through the plant canopy. The Spectra Vista spectroradiometer is a downward-viewing instrument that is strongly affected by the reflectance of background water and soil visible through the plant canopy.

For example, in habitat type D1, prostrate evergreen shrubs (dominated by *Dryas integrifolia*) composed an average of 54 ±14 percent of total biomass (Figure 12). Other low-stature growth forms including lichens, bryophytes, and litter, collectively composed an average of another 38 percent. As a result, an average of approximately 92 percent of total biomass in D1 was potentially not viewable by the LAI-2000 sensors; whereas nearly all of the D1 biomass can be viewed by the NDVI sensors. This accounts for the large difference between LAI and NDVI values for dry tundra. Similar patterns are seen in other dry and moist types (Dsn, Dz, and M1), where prostrate evergreen dwarf shrubs contribute a large component of total biomass. A similar problem occurs in aquatic types, where much of the biomass is below the water surface (A1t, A2, A3t, and A4t). It is less of a problem where taller graminoids are viewed by the sensors of both the LAI and NDVI instruments (types Mz, M3, A1 W2).

As discussed, NDVI values were depressed in aquatic sites where the majority of the biomass is below water. Several NDVI values obtained from aquatic habitats (e.g., types L3, A3t, and A4t) were negative. Aquatic plots with relatively large components of floating or emergent biomass (types A1, A1t, A2, A3t) had relatively high NDVI values. The aquatic moss type A3t (dominated by *Calliergon richardsonii*) had extreme high mean biomass (over 3500 g m^{-2}) that was not reflected in either the LAI or NDVI data. However, NDVI for type A3t was relatively high compared to most other aquatic types due to the floating mats of moss detectable by the instrument's sensors.

3.2 Trends of NDVI vs. LAI

Overall, NDVI increased logarithmically with respect to LAI for the full dataset (Figure 13), similar to the NDVI-LAI relationship observed for datasets along the full Arctic bioclimate gradient in Arctic Russia (Epstein et al. 2021). NDVI begins to saturate at LAI values above approximately 0.4. NDVI vs. LAI have mixed trends for the four site-moisture groups (Figure 13b) and the groups of plots on different surface features (Figure 13c). The NDVI vs. LAI trends for the wet and aquatic plots most closely match the trend for all plots.

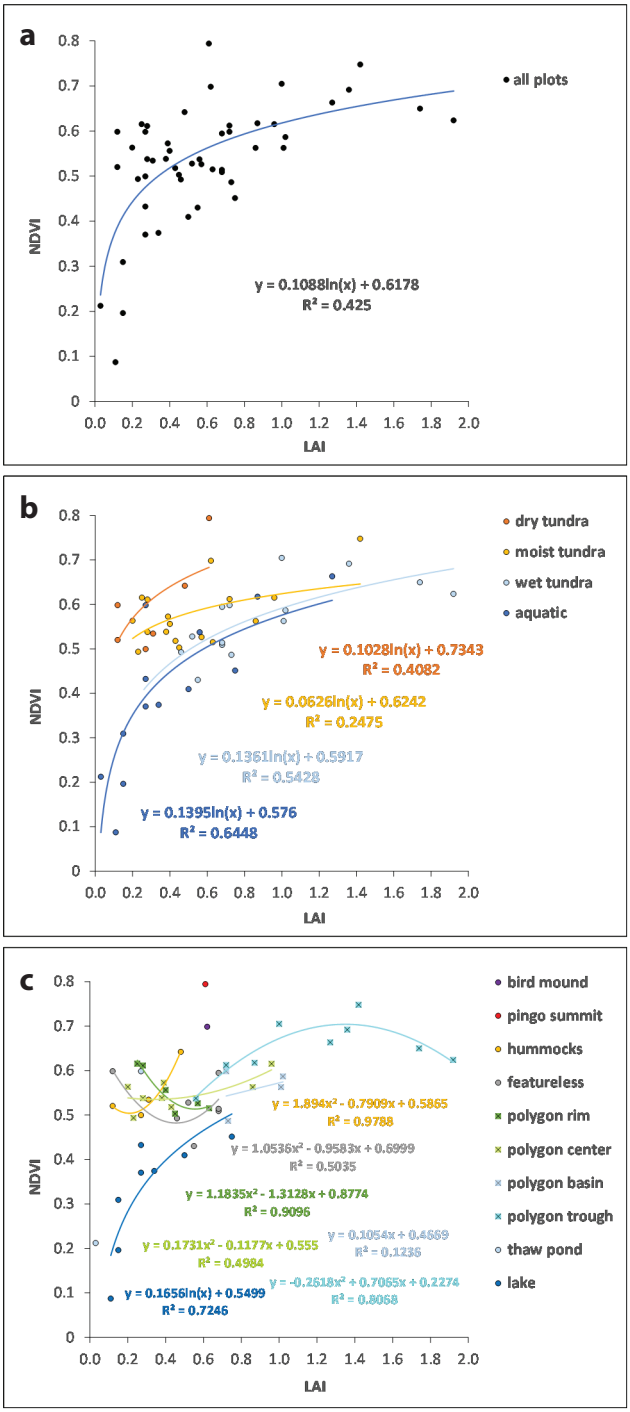

Figure 13. *NDVI vs. LAI.* ***a.*** *All plots;* ***b.*** *site-moisture groups;* ***c.*** *surface features. Best-fit trend lines are shown for groups with more than three plots. LAI values of 0, NDVI values ≤0, and groups with <3 values were removed from the analysis.*

3.3 Colleen and Airport plots

LAI and NDVI data from the nearby Colleen and Airport sites are presented in Appendix Table A2 including plot characterization, vegetation height, and water-cover data that were collected at the same time.

The data from these sites are presented without analysis because of differences between the Colleen and Airport datasets compared to the data collected at the NIRPO site:

- No biomass data have been collected from the Colleen or Airport sites to compare with the NIRPO data.
- LAI data were collected but in different years and using different instrumentation than used at the NIRPO site. LAI data were collected from Colleen plots and at 1-m intervals along transects T1 and T2 in 2014 and from the Airport plots and transects T3 and T4 in 2016 using an AccuPAR LP-80 PAR/LAI Ceptometer®. LAI data for the Colleen site are in AGC Data Report 15-01 Tables 2.1A, 2.1B, 2.2A and 2.2B (Walker et al. 2015). LAI data for the Airport site are in AGC Data Report 16-01, Tables 3.1A, 3.1B, 3.2A and 3.2B (Walker et al. 2016)
- Field spectroscopy data were collected from the Airport plots and transects in 2015 using a Spectral Evolution PSR+3500® full range spectrometer that measures reflected surface radiance in the region from 345 to 2507 nm in 6-8 nm channels. Full spectral signatures from the 20 center and trough plots along T3 and T4 are in AGC Data Report 16-01, Fig. 2.9 (Walker et al. 2016). NDVI values were calculated for points at 1-m intervals along Transects T3 and T4 and for the 20 center and trough plots (Walker et al. 2016, Tables 3.1A, 3.1B, 3.2A and 3.2B).
- Preliminary analysis of the Colleen LAI data were presented in posters at the Arctic Change 2014 meeting in Ottawa, Canada (Raynolds et al. 2014) and the XI International Conference on Permafrost in Postdam, Germany (Buchhorn et al. 2016b).

An analysis of the LAI and NDVI data from the roadside plots at the Colleen and Airport sites in comparison with plots in comparable vegetation types at the NIRPO site would be useful for studies using remote sensing tools to examine the cumulative effects of roads on adjacent tundra areas.

4 Conclusions

The vegetation of the Prudhoe Bay region is changing rapidly due to the warming climate, increasing abundance of erect shrubs, changes in the abundance and distribution of water, and infrastructure-related factors, especially near roads and gravel pads. This data report and preliminary analysis focused on 59 permanent vegetation plots within the 0.88 km^2 NIRPO site. The vegetation at the NIRPO site is representative of the nonacidic calcareous tundra found in thaw lake plain landscapes downwind of the Sagavanirktok River at the northern edge of Bioclimate Subzone D (CAVM Team 2003).

The vegetation classification (Table 1) included the classification includes four broad site-moisture categories (dry tundra, moist tundra, wet tundra, and aquatic vegetation) subdivided into 28 finer level vegetation habitats. The full legend is being used for ongoing efforts to classify and map the vegetation of the NNA-IRPS study site.

A conceptual site-moisture gradient for the NIRPO site was constructed by arranging 17 vegetation habitats that occurred in the sampled plots according to subjective site-moisture scores determined in the field during the plot surveys (Table 2) and the mean volumetric soil-moisture values determined from soil samples of the top mineral soil horizons of each plot. Key site and vegetation factors all showed differing trends across the conceptual site-moisture gradient. Thaw depth peaked in the dry types. Vegetation height peaked in the wet and aquatic types. Water depth and snow depth peaked in the aquatic types. LAI peaked in wet tundra (especially W1) with secondary peaks in moist and aquatic transitional types (M3t and A1t) also near the center of the site-moisture gradient. NDVI values were relatively high across dry, moist, and wet site-moisture groups and lowest in the aquatic plots where most of the biomass was below water (Figure 12).

Aboveground biomass of individual plant growth forms also had maxima in different parts of the gradient (Figure 11). Total biomass was greatest in transitional aquatic moss plant communities in thermokarst ponds (type A3t, 4.7 kg m^{-2}, N = 3). This value included communities dominated by *Scorpidium scorpioides* and *Calliergon richardsonii* and far exceeded values from all the other vegetation habitats in the Prudhoe Bay region. The high values need to be confirmed with more samples from similar thermokarst-pond communities elsewhere.

The instruments used for collecting the LAI and NDVI data both have limitations for accurately reflecting trends in biomass. The LAI-2000 instrument misses the biomass of very low-growing plants, including most mosses, lichens, prostrate dwarf shrubs, litter, and many small forbs because of its elevated sensor. This is a problem especially in dry tundra where these growth forms compose the majority of the biomass, and there is low cover of taller growth forms.

Currently, erect deciduous shrubs do not contribute large amounts of biomass in any of the plots sampled at the NIRPO site due to the cold coastal summer climate (Figures 10). Deciduous-shrub biomass averaged only 6.7 ± 9 percent of the total biomass for moist tundra types and less than 2 percent for dry, wet, and aquatic vegetation. Nearly all this was contributed by prostrate dwarf shrubs (e.g., *Salix arctica, S. reticulata, S. rotundifolia, S. ovalifolia*). Dense patches of erect willows, mainly *Salix lanata*, occur in some streamside sites within the Prudhoe Bay oilfield and on some heavily disturbed sites along roads, such as disturbed trenches of buried communication cables. On undisturbed dry, mesic, and wet habitats, erect willows are generally sparsely distributed within the oilfield. However, erect deciduous shrub abundance is rapidly changing in the region as the climate warms and in response to infrastructure-related disturbances that warm the soil (Walker et al. 2022b).

It would be useful to periodically conduct similar surveys supplemented with photos to document the increase in erect shrubs within the oilfield and in other bioclimate subzones along the Dalton Highway. Satellite and drone-based remote-sensing methods are the only practical way to monitor changes over long periods of time, but baseline ground information is essential to interpreting the data obtained from aerial sensors.

5 References

Asner, G. P. 1998. Biophysical and biochemical sources of variability in canopy reflectance. Remote sensing of environment **64**:234–253.

Bergstedt, H., Jones, B. M., Walker, D. A., Peirce, J. L., Bartsch, A., Pointner, G., Kanevskiy, M. Z., Raynolds, M. K., and Buchhorn, M. 2023. The spatial and temporal influence of infrastructure and road dust on seasonal snowmelt, vegetation productivity, and early season surface water cover in the Prudhoe Bay Oilfield. Arctic Science **9**:243–259.

Bhatt, U. S., Walker, D. A., Raynolds, M. K., Comiso, J. C., Epstein, H. E., Jia, G., Gens, R., Pinzon, J. E., Tucker, C. J., Tweedie, C. E., and Webber, P. J. 2010. Circumpolar Arctic tundra vegetation change is linked to sea -ice decline. Earth Interactions **14**:1–20.

Bliss, L. C. 1997. Arctic ecosystems of North America. Pages 551–683 *in* F. E. Wielgolaski, editor. Polar and Alpine Tundra. Elesevier, Amsterdam, Netherlands.

Buchhorn, M., Walker, D. A., Heim, B., Raynolds, M. K., Epstein, H. E., and Schwieder, M. 2013. Ground-based hyperspectral characterization of Alaska tundra vegetation along environmental gradients. Remote Sensing **5**:3971–4005.

Buchhorn, M., Raynolds, M. K., and Walker, D. A. 2016a. Influence of BRDF on NDVI and biomass estimations of Alaska Arctic tundra. Environmental Research Letters **11**:125002.

Buchhorn, M., Raynolds, M. K., Kanevskiy, M., Matyshak, G., Shur, Y., Willis, M. D., Peirce, J. L., Wirth, L. M., and Walker, D. A. 2016b. Effects of 45 years of heavy road traffic and climate change on the thermal regime of permafrost and tundra at Prudhoe Bay, Alaska. Pages 1203–1205 *in* F. Gunther and A. Morgenstern, editors. XI. International Conference on Permafrost—Book of Abstracts, Potsdam, Germany, 20-24 June 2016. Bibliothek Wissenschaftspark Albert Einstein, Potsdam, Germany.

CAVM Team 2003. Circumpolar Arctic Vegetation Map. Conservation of Arctic Flora and Fauna (CAFF) Map No. 1. U.S. Fish & Wildlife Service, Anchorage, Alaska, USA.

Davies, C. E., Moss, D., and Hill, M. O. 2004. EUNIS Habitat Classification Revised 2004. Report to the European Environment Agency, European Topic Centre on Nature Protection and Biodiversity.

Epstein, H. E., Walker, D. A., Raynolds, M. K., Jia, G. J., and Kelley, A. M. 2008. Phytomass patterns across a temperature gradient of the North American arctic tundra. Journal of Geophysical Research: Earth Surface **113**:1748.

Epstein, H., Walker, D., Frost, G., Raynolds, M., Daanen, R., Forbes, B., Geml, J., Kaärlejarvi, E., Khitun, O., Khomutov, A., Kuss, P., Leibman, M., Matyshak, G., Moskalenko, N., Orekhov, P., Romanovsky, V., and Timling, I. 2021. Spatial patterns of arctic tundra vegetation properties on different soils along the Eurasia Arctic Transect, and insights for a changing Arctic. Environmental Research Letters **16**:014008.

Everett, K. R., and Parkinson, R. J. 1977. Soil and landform associations, Prudhoe Bay area, Alaska. Arctic and Alpine Research **9**:1–19.

Everett, K. R. 1980. Landforms. Pages 14–20 in Geobotanical Atlas of the Prudhoe Bay Region, Alaska, CRREL Report 80-14. U.S. Army, Cold Regions Research and Engineering Laboratory, Hanover, New Hampshire, USA.

Frost, G. V., Christopherson, T., Jorgenson, M. T., Liljedahl, A. K., Macander, M. J., Walker, D. A., and Wells, A. F. 2018. Regional patterns and asynchronous onset of ice-wedge degradation since the mid-20th century in Arctic Alaska. Remote Sensing **10**:1312.

Frost, G. V., Macander, M. J., Bhatt, U. S., Berner, L., Bjerke, J. W., Epstein, H. E., Forbes, B. C., Goetz, S. J., Lara, M. J., Phoenix, G. K., Serbin, S. P., Tømmervik, H., Walker, D. A., and Lang, D. 2022. Tundra greenness *in* M. L. Druckenmiller, R. L. Thoman, and T. A. Moon, editors. Arctic Report Card 2022.

Heijmans, M. M. P. D., Magnússon, R. Í., Lara, M. J., Frost, G. V., Myers-Smith, I. H., van Huissteden, J., Jorgenson, M. T., Fedorov, A. N., Epstein, H. E., Lawrence, D. M., and Limpens, J. 2022. Tundra vegetation change and impacts on permafrost. Nature Reviews Earth & Environment **3**:68–84.

Hope, A., Engstrom, R., and Stow, D. 2005. Relationship between AVHRR surface temperature and NDVI in

Arctic tundra ecosystems. International Journal of Remote Sensing **26**:1771–1776.

Jespersen, R. G., Anderson-Smith, M., Sullivan, P. F., Dial, R. J., and Welker, J. M. 2023. NDVI changes in the Arctic: functional significance in the moist acidic tundra of Northern Alaska. PLOS ONE **18**:e0285030.

Jorgenson, M. T., Shur, Y. L., and Pullman, E. R. 2006. Abrupt increase in permafrost degradation in Arctic Alaska. Geophysical Research Letters **25**:L02503.

Jorgenson, M. T., Kanevskiy, M. Z., Jorgenson, J. C., Liljedahl, A., Shur, Y., Epstein, H. E., Kent, K., Griffin, C. G., Daanen, R., Boldenow, M., Orndahl, K., Witharana, C., and Jones, B. M. 2022. Rapid transformation of tundra ecosystems from ice-wedge degradation. Global and Planetary Change **216**:103921.

Kanevskiy, M., Shur, Y., Jorgenson, T., Brown, D. R. N., Moskalenko, N., Brown, J., Walker, D. A., Raynolds, M. K., and Buchhorn, M. 2017. Degradation and stabilization of ice wedges: Implications for assessing risk of thermokarst in northern Alaska. Geomorphology **297**:20–42.

Kanevskiy, M., Shur, Y., Walker, D. A., Jorgenson, T., Raynolds, M. K., Peirce, J. L., Jones, B. M., and Buchhorn, M. 2022. The shifting mosaic of ice-wedge degradation and stabilization in response to infrastructure and climate change, Prudhoe Bay oilfield, Alaska, USA. Arctic Science **8**:498-530.

Komárková, V. 1983. Comparison of habitat type classification to some other classification methods. Pages 21-31 *in* W. H. Moir and L. Hendzel, editors. Proceedings of the Workshop on Southwestern Habitat Types, Albuquerque, New Mexico, 6–8 April 1983. U.S. Department of Agriculture Forest Service, Southwestern Region.

LI-COR Inc. 1992. LAI-2000 plant canopy analyzer operating manual. LI-COR, Inc.

Mucina, L., Bültmann, H., Dierssen, K., Theurillat, J. P., Raus, T., Carni, A., Sumberova, K., Willner, W., Dengler, J., Garcia, R. G., Chytry, M., Hájek, M., Pietro, R. D., Iakushenko, D., Pallas, J., Daniëls, F. J. A., Bergmeier, E., Guerra, A. S., Ermakov, N., … and L. Tichý. 2016. Vegetation of Europe: Hierarchical floristic classification system of vascular plant, bryophyte, lichen, and algal communities. Applied Vegetation Science **19**:3–264.

Myers-Smith, I. H., Hallinger, M., Blok, D., Sass-Klaassen, U., Rayback, S. A., Weijers, S., Trant, A. J., Tape, K. D., Naito, A. T., Wipf, S., Rixen, C., Dawes, M. A., Wheeler, J. A., Buchwal, A., Baittinger, C., Macias-Fauria, M., Forbes, B. C., Lévesque, E., Boulanger-Lapointe, N., … and Wilmking, M. 2015. Methods for measuring arctic and alpine shrub growth: A review. Earth Science Reviews **140**:1–13.

Rawlinson, S. E. 1993. Surficial geology and morphology of the Alaskan central Arctic coastal plain. Report of Investigations, 93-1. Alaska Division of Geology and Geophysical Surveys, Fairbanks, Alaska, USA.

Raynolds, M. K., Walker, D. A., and Maier, H. A. 2006. NDVI patterns and phytomass distribution in the circumpolar Arctic. Remote Sensing of Environment **102**:271–281.

Raynolds, M. K., Walker, D. A., Epstein, H. E., Pinzon, J. E., and Tucker, C. J. 2011. A new estimate of tundra-biome phytomass from trans-Arctic field data and AVHRR NDVI. Remote Sensing Letters **3**:403–411.

Raynolds, M. K., Walker, D. A., Buchhorn, M., and Wirth, L. 2014. Vegetation changes related to 45 years of heavy road traffic along the Spine Road at Prudhoe Bay, Alaska. Poster Abstract 333. Arctic Change, Ottowa, Ontario, Canada, 8–12 December 2014.

Raynolds, M. K., and Walker, D. A. 2016. Increased wetness confounds landsat-derived NDVI trends in the central Alaska North Slope region, 1985–2011. Environmental Research Letters **11**:085004.

Schickhoff, U., Walker, M. D., and Walker, D. A. 2002. Riparian willow communities on the Arctic Slope of Alaska and their environmental relationships: A classification and ordination analysis. Phytocoenologia **32**:145–204.

Shippert, M. M., Walker, D. A., Auerbach, N. A., and Lewis, B. E. 1995. Biomass and leaf-area index maps derived from SPOT images for Toolik Lake and Imnavait Creek areas, Alaska. Polar Record **31**:147–154.

Shur, Y., Kanevskiy, M., Walker, D. A., Jorgensen, T., Buchhorn, M., Raynolds, M. K., and Toniolo, H. 2016. Permafrost-related causes and consequences of the Sagavanirktok River Delta flooding in spring 2015. Pages 1014–1016 *in* F. Gunther and A. Morgenstern, editors. XI. International Conference on Permafrost—Book of Abstracts, Potsdam, Germany, 20-24 June 2016. Bibliothek Wissenschaftspark Albert Einstein, Potsdam, Germany.

Stow, D. A., Hope, A., McGuire, D., Verbyla, D., Gamon, J., Huemmrich, F., Houston, S., Racine, C., Sturm, M., Tape, K., Hinzman, L., Yoshikawa, K., Tweedie, C., Noyle, B., Silapaswan, C., Douglas, D., Griffith, B., Jia, G., Epstein, H., … and Myneni, R. 2004. Remote sensing of vegetation and land-cover change in Arctic tundra ecosystems. Remote Sensing of Environment **89**:281–308.

Toniolo, H., Stutzke, J., Lai, A., Youcha, E., Tschetter, T., Vas, D., Keech, J., and Irving, K. 2017. Antecedent conditions and damage caused by 2015 spring flooding on the Sagavanirktok River, Alaska. Journal of Cold Regions Engineering **31**:05017001.

van Everdingen, R. (editor). 2005. Multi-language glossary of permafrost and related ground-ice terms. International Permafrost Association, Arctic Institute of North America, Calgary, Alberta, Canada.

Walker, D. A., Everett, K. R., Webber, P. J., and Brown, J. 1980. Geobotanical atlas of the Prudhoe Bay Region, Alaska, CRREL Report 80-14. U.S. Army, Cold Regions Research and Engineering Laboratory, Hanover, New Hampshire, USA.

Walker, D. A. 1985. Vegetation and environmental gradients of the Prudhoe Bay region, Alaska. CRREL Report 85-14. U.S. Army, Cold Regions Research and Engineering Laboratory, Hanover, New Hampshire, USA.

Walker, D. A., and Everett, K. R. 1991. Loess ecosystems of northern Alaska: Regional gradient and toposequence at Prudhoe Bay. Ecological Monographs **61**:437–464.

Walker, D. A., Buchhorn, M., Kanevskiy, M., Matyshak, G. V., Raynolds, M. K., Shur, Y. L., and Peirce, J. L. 2015. Infrastructure-thermokarst-soil-vegetation interactions at Lake Colleen site A, Prudhoe Bay, Alaska. AGC Data Report 15-01. Alaska Geobotany Center, University of Alaska Fairbanks, Fairbanks, Alaska, USA.

Walker, D. A., Buchhorn, M., Kanevskiy, M., Raynolds, M. K., Shur, Y. L., and Wirth, L. M. 2016. Road effects at Airport study site, Prudhoe Bay, Alaska, summer 2015. AGC Data Report 16-01. Alaska Geobotany Center, University of Alaska Fairbanks, Fairbanks, Alaska, USA.

Walker, D. A., Kanevskiy, M., Raynolds, M. K., and Peirce, J. L. 2018a. 2016 ArcSEES data report: Snow, thaw, temperature and permafrost borehole data from the Colleen and Airport sites, Prudhoe Bay, Alaska, and Quintillion fiber optic cable impacts, North Slope, Alaska. AGC Data Report 18-01. Alaska Geobotany Center, University of Alaska Fairbanks, Fairbanks, Alaska, USA.

Walker, D. A., Daniëls, F. J. A., Matveyeva, N. V., Šibík, J., Walker, M. D., Breen, A. L., Druckenmiller, L. A., Raynolds, M. K., Bültmann, H., Hennekens, S., Buchhorn, M., Epstein, H. E., Ermokhina, K., Fosaa, A. M., Heiðmarsson, S., Heim, B., Jónsdóttir, I. S., Koroleva, N., Lévesque, E., … and Wirth, L. M. 2018b. Circumpolar Arctic Vegetation Classification. Phytocoenologia **48**:181–201.

Walker, D. A., Kanevskiy, M., Breen, A. L., Kade, A., Daanen, R. P., Jones, B. M., Nicolsky, D. J., Bergstedt, H., Watson-Cook, E., and Peirce, J. L. 2022a. Observations in ice-rich permafrost systems, Prudhoe Bay, Alaska, 2020–2021. AGC Data Report 22-01. Alaska Geobotany Center, University of Alaska Fairbanks, Fairbanks, Alaska, USA.

Walker, D. A., Raynolds, M. K., Kanevskiy, M. Z., Shur, Y. S., Romanovsky, V. E., Jones, B. M., Buchhorn, M., Jorgenson, M. T., Šibík, J., Breen, A. L., Kade, A., Watson-Cook, E., Matyshak, G., Bergstedt, H., Liljedahl, A. K., Daanen, R. P., Connor, B., Nicolsky, D., and Peirce, J. L. 2022b. Cumulative impacts of a gravel road and climate change in an ice-wedge-polygon landscape, Prudhoe Bay, Alaska. Arctic Science **8**:1040–1056.

Walker, D. A., Peirce, J. L., Bergstedt, H., Breen, A. L., Daanen, R., Hobgood, O., Jones, B. J., Kade, A., Kučerová, A., Liljedahl, A. K., Manos, E., Nicolsky, D. M., Peirce, J. L., Raynolds, M. K., Romanovsky, V. E., Rybakov, S., Shur, Y. L., Watson-Cook, E., and Witharana, C. 2023. Natural ice-rich permafrost observatory, Prudhoe Bay, Alaska: 2022 field activities. AGC Data Report 23-02. Alaska Geobotany Center, University of Alaska Fairbanks, Fairbanks, Alaska, USA.

Watson-Cook, E. 2022. Thermokarst-pond plant community characteristics and effects on ice-wedge degradation in the Prudhoe Bay region. M.S. thesis. University of Alaska Fairbanks, Fairbanks, Alaska, USA.

Webber, P. J. 1978. Spatial and temporal variation in the vegetation and its productivity, Barrow, Alaska. Pages 37–112 *in* L. L. Tieszen, editor. Vegetation and Production Ecology of an Alaskan Arctic Tundra. Springer Verlag, New York, New York, USA.

Webber, P. J., and Walker, D. A. 1975. Vegetation and landscape analysis at Prudhoe Bay, Alaska: A vegetation map of the Tundra Biome study area. Pages 81–91 *in* J. Brown, editor. Ecological Investigations of the Tundra Biome in the Prudhoe Bay Region, Alaska. Biological Papers of the University of Alaska, Special Report Number 2. U.S. Army, Cold Regions Research and Engineering Laboratory, Hanover, New Hampshire, USA.

Zwieback, S., McClernan, M., Kanevskiy, M., Jorgenson, M. T., Walker, D. A., Chang, Q., Bergstedt, H., Toniolo, H., Romanovsky, V. E., Meyer, F. J. 2023. Disparate permafrost terrain changes after a large flood observed from space. Permafrost and Periglacial Processes **34**:451–466.

APPENDIX 1 Key plot data for 59 NIRPO plots

Table A1. *Key plot data for 59 NIRPO plots where NDVI and LAI were collected, 19–21 July 2023. Plots are grouped according to subjective site-moisture status (dry – pink; moist – yellow; wet – light blue; aquatic – dark blue). Abbreviated legends for landscape characterization are in Table 1. Surface geology codes are from Rawlinson (1993). NDVI measurements were recorded by Kelcy Kent and Amy Breen using a Spectra Vista Corporation (SVC) i-Series field-portable spectroradiometer, model HR-1024i (Figure 8). LAI observations were made by Skip Walker and Helga Bültmann using a LiCOR LAI 2000 instrument (Figure 7). Vegetation height was collected at the same time. Aboveground biomass was harvested 24–30 August 2021, except for plots 22-01 to 22-15 (indicated by *), which were sampled 26–31 August 2022. Thaw and water depths were measured during 23–26 August 2023, and snow depth was measured between 30 April–5 May 2024. Mean ground surface temperature, thawing degree days (TDD) and freezing degree days (FDD) were calculated from Thermocron iButton temperature measurements recorded every 4 hours between 15 September 2022 and 20 August 2023. At plots where two iButtons were deployed at the ground surface over the same time period, mean temperature values were used. NA = not available or not assessed.*

		Plot characterization					NDVI		LAI			Vegetation ht.					Surface temperature		
Plot ID	Transect	Surficial geology	Landform	Surface feature	Surface-feature element	Vegetation habitat	Mean	SE	Mean	SE	Total biomass (g/m²)	Mean (cm)	SD	Thaw depth (cm)	Water depth (cm)	Snow depth (cm)	Mean (° C)	FDD	TDD
22-01	LP	Qti	P	N	n	D1	0.54	0.04	0	0	915*	2	1	130	0	5	-7.5	-2033	210
22-02	LP	Qti	P	N	n	D1	0.57	0.02	0	0	760*	2	0.6	130	0	9	-7.4	-2386	258
22-03	LP	Qti	P	N	n	D1	0.60	0.04	0.12	0.05	812*	2	1	125	0	5	NA	NA	NA
22-04	LP	Qti	P	H	n	D2	0.52	0.01	0.12	0.04	957*	2	1	125	0	34	-4.4	-1882	711
22-05	LP	Qti	P	H	n	D2	0.50	0.04	0.27	0.10	1298*	4	1.6	126	0	27	-6.2	-2381	395
22-06	LP	Qti	P	H	n	D2	0.53	0.01	0.31	0.02	586*	5	2.2	108	0	30	NA	NA	NA
22-13	LP	Qti	P	Z	n	Dz	0.79	0.01	0.61	0.07	825*	7	0.5	82	0	4	-7.4	-2377	773
22-14	LP	Qti	P	H	n	Dsn	0.64	0.01	0.48	0.24	1384*	6	1.3	121	0	54	-5.2	-2747	771
21-05	T6	Qsg	R	HCP1	c	M1	0.57	0.02	0.39	0.09	924	13	2.4	58	0	29	-5.8	-2174	50
21-06	T6	Qsg	R	HCP1	c	M1	0.56	0.02	0.2	0.07	1019	7	2.6	53	0	15	-6.7	-1000	18
21-07	T6	Qsg	R	HCP1	c	M3	0.62	0.01	0.96	0.24	997	17	1.7	54	0	21	-5.0	-1856	409
21-08	T6	Qsg	R	TP2	c	M3t	0.56	0.01	0.86	0.06	875	17	3	52	0	36	-4.7	-1990	11
21-09	T6	Qsg	R	TP2	c	M3t	0.52	0.01	0.43	0.06	1087	12	2.1	55	0	29	-4.9	-2413	68
21-10	T6	Qsg	R	TP2	r	M1	0.56	0.01	0.4	0.08	1697	8	2.1	50	0	30	-5.4	-3671	973
21-11	T6	Qsg	R	TP2	t	M3t	0.75	0.01	1.42	0.09	515	27	3.9	49	7	59	-4.3	-2462	521
21-15	T6	Qsg	R	HCP1	t	M3t	0.61	0.01	0.72	0.13	1250	16	2.7	42	0	70	-3.9	-2402	723
21-17	T8	Qti	DLir1	DP	r	M3	0.52	0.01	0.63	0.14	996	16	3	55	0	33	-5.0	-2956	560
21-18	T8	Qti	DLir1	DP	r	M3	0.53	0.01	0.57	0.04	641	14	2.9	48	0	41	-4.7	-2320	394
21-20	T9	Qsg	R	HCP1	c	M1	0.49	0.00	0.23	0	1292	6	2.2	48	0	14	-5.9	-2762	842
21-21	T9	Qsg	R	HCP2	c	M1	0.54	0.01	0.38	0.05	1252	8	2.6	49	0	14	-6.6	-2143	110
21-22	T9	Qsg	R	HCP2	c	M1	0.54	0.01	0.28	0.06	1171	9	1	43	0	28	-5.5	-2198	729
21-24	T9	Qti	DLir1	DP	r	M1	0.50	0.01	0.45	0.15	1083	7	1.2	48	0	21	-5.6	-2127	95
21-30	T7	Qti	DLir2	LCP1	r	M3	0.61	0.02	0.28	0.02	1025	9	2.5	57	0	32	NA	NA	NA
21-34	T7	Qti	DLir2	LCP1	r	M3	0.62	0.01	0.25	0.02	534	11	1.9	57	0	38	-5.5	-2205	73
22-15	T8	Qti	DLir1	BM	n	Mz	0.70	0.01	0.62	0.09	886*	13	2.1	43	0	12	-7.9	-2646	542
21-01	T8	Qti	DLir1	DP	n	W1	0.51	0.01	0.68	0.12	658	14	1.4	50	1	49	-5.2	-2277	396
21-02	T8	Qti	DLir1	DP	n	W1	0.53	0.01	0.52	0.06	400	12	1	56	4	15	-4.9	-2344	315
21-03	T8	Qt	DLip	N	n	W2	0.43	0.03	0.55	0.1	159	14	3	53	4	23	-5.5	-1911	184
21-04	T8	Qt	DLip	N	n	W2	0.49	0.03	0.46	0.04	688	19	5.7	51	5	36	-5.6	-2793	474

Table A1.1 *(continued)*

Plot ID	Transect	Plot characterization					NDVI		LAI		Total biomass (g/m^2)	Vegetation ht.		Thaw depth (cm)	Water depth (cm)	Snow depth (cm)	Surface temperature		
		Surficial geology	Land-form	Surface feature	Surface-feature element	Vege-tation habitat	Mean	SE	Mean	SE		Mean (cm)	SD				Mean (° C)	FDD	TDD
21-12	T6	Qsg	R	LCP2	t	W1	0.69	0.02	1.36	0.17	616	21	3.3	48	4	48	-3.4	-3170	546
21-13	T6	Qsg	R	HCP1	t	W1	0.62	0.00	1.92	0.12	315	22	5	51	2	61	NA	NA	NA
21-14	T6	Qsg	R	HCP1	t	W1	0.65	0.03	1.74	0.1	888	28	5	47	14	55	-3.4	-2379	795
21-16	T6	Qsg	R	TP1	t	W1	0.70	0.02	1	0.15	784	26	1.5	48	15	55	-4.9	-2374	406
21-19	T9	Qti	DLir1	DP	n	W2	0.51	0.00	0.68	0.12	520	16	1.2	53	1	36	NA	NA	NA
21-23	T9	Qti	DLir1	DP	n	W1	0.59	0.01	0.68	0.09	894	14	1.3	53	1	43	-4.7	-2123	103
21-27	T7	Qti	DLir2	LCP1	b	W1	0.49	0.01	0.73	0.1	212	19	1.7	62	0	38	-4.1	-2368	884
21-28	T7	Qti	DLir2	LCP1	b	W2	0.56	0.01	1.01	0.04	241	25	2.8	56	8	42	-4.5	-3047	273
21-29	T7	Qti	DLir2	LCP1	b	W1	0.59	0.01	1.02	0.21	649	23	3.3	63	2	35	-4.9	-3033	805
21-33	T7	Qti	DLir2	LCP2	b	W2	0.60	0.03	0.72	0.12	286	26	2.5	66	11	46	NA	NA	NA
21-25	T7	Qti	L2	L2	n	L2	0.20	0.01	0.15	0.05	18	11	2.5	58	0	40	-5.1	-2795	60
21-26	T7	Qti	L2	L2	n	L2	0.31	0.03	0.15	0.06	32	11	1.2	61	0	37	NA	NA	NA
21-31	T7	Qti	DLir2	LCP2	t	A1t	0.54	0.01	0.56	0.02	479	24	3	50	17	44	-5.4	-3535	995
21-32	T7	Qti	DLir2	LCP1	t	A1t	0.66	0.02	1.27	0.15	564	26	1.3	50	9	74	NA	NA	NA
21-35	T7	Qti	DLir2	LCP2	t	A1t	0.62	0.04	0.87	0.16	322	28	6.5	46	22	38	-5.1	-2928	324
21A-22	T6	Qau	L3	L3	n	A4t	-0.15	0.03	0	0	167	0	0	57	51	89	NA	NA	NA
21A-26	T6	Qau	L3	L3	n	A3t	0.21	0.15	0.03	0	4702	1	0.5	42	48	60	-4.1	-2304	248
21A-27	T6	Qau	L3	L3	n	L3	-0.21	0.01	0	0	486	0	0	56	53	54	-3.0	-2301	272
21A-28	T6	Qau	L3	L3	n	A4t	-0.14	0.07	0.26	0.07	396	7	1.4	50	40	59	-3.3	-2149	247
21A-29	T6	Qau	L3	L3	n	A3t	-0.25	0.02	0	0	6074	0	0	42	52	60	NA	NA	NA
21A-35	T6	Qau	L3	L3	n	L3	-0.30	0.03	0	0	154	0	0	52	53	93	-2.3	-2220	272
21A-36	T6	Qau	L3	L3	n	A3t	0.60	0.08	0.27	0.04	3735	2	0.5	42	35	90	NA	NA	NA
21A-38	T6	Qau	L3	L3	n	L3	-0.32	0.01	0	0	86	0	0	51	62	70	NA	NA	NA
21A-40	T6	Qau	L3	L3	n	A4t	-0.14	0.10	0	0	84	0	0	50	57	56	NA	NA	NA
22-07	LP	Qti	L2	L2	n	A1	0.45	0.03	0.75	0.06	199*	26	2.9	59	4	45	NA	NA	NA
22-08	LP	Qti	L2	L2	n	A1	0.43	0.03	0.27	0.17	140*	31	4.3	60	10	34	-4.8	-1824	293
22-09	LP	Qti	L2	L2	n	A1	0.37	0.06	0.27	0.06	464*	31	1.7	61	20	37	-4.1	-3030	755
22-10	LP	Qti	L2	L2	n	A2	0.09	0.04	0.11	0.04	158*	19	2.5	43	60	47	NA	NA	NA
22-11	LP	Qti	L2	L2	n	A2	0.37	0.06	0.34	0.03	1178*	24	1.2	52	40	39	NA	NA	NA
22-12	LP	Qti	L2	L2	n	A2	0.41	0.05	0.5	0.09	907*	20	3.7	52	24	44	-4.8	-2093	757

APPENDIX 2 Key data for Colleen and Airport Site plots

Table A2. *Key data from the roadside plots at the Colleen site (transects T1 and T2, 27 August 2023) and Airport site (transects T3, T4, and T5, 23 August 2023). Plot landscape characterization for surficial geology, landform, and surface features considers the original landscapes before road disturbance as interpreted from aerial photographs (U.S. Navy 1949, BAR). Vegetation habitat was characterized during the 2023 survey using the vegetation habitat codes in Table 1. NDVI data were collected July 22–23, 2023 by Kelcy Kent and Amy Breen using a Spectravista, HR-1024i (Figure 8). LAI, vegetation height, and water depth data were collected 19–21 July 2023 by Skip Walker and Helga Bültmann using a LiCOR LAI 2000 Plant Canopy Analyzer (Figure 7). NA = not available or not assessed.*

		Plot landscape characterization[1]					NDVI		LAI						
Plot ID	Transect	Surficial geology	Landform	Surface feature	Surface-feature element	Vegetation habitat	File number	Mean	SE	Mean	SE	Veg height[2] (cm)	Water depth (cm)	Photo number	Notes[3]
T1-5-C	T1	Qsg	R	TP1	c	M3d	72	0.48	0.02	1.34	0.8	14	0	1595-96	
T1-5-T	T1	Qsg	R	TP1	t	W1d	73	0.63	0.02	1.34	0.08	25	0	1597-98	1st LAI: 1.52 ± 0.16
T1-10-C	T1	Qsg	R	TP1	c	M3d	74	0.51	0.02	0.5	0.06	17	0	1599-1600	lcp basin
T1-10-T	T1	Qsg	R	TP1	t	W1d	75	0.53	0.01	0.99	0.08	21	3	1601	lcp trough
T1-25-C	T1	Qsg	R	LCP1	c	M3d	77	0.49	0.03	0.35	0.07	11	0	1604-06	lcp basin
T1-25-T	T1	Qsg	R	TP1	t	W1d	76	0.67	0.02	1.34	0.11	31	13	1602-03	
T1-50-C	T1	Qsg	R	TP1	c	M3d	79	0.50	0.02	0.33	0.07	10	0	1610-11	SALLAN to 18 cm
T1-50-T	T1	Qsg	R	TP1	t	W1d	78	0.06	0.03	NA	NA	10	28	1607-09	Thermokarst pond with SCOSCO
T1-100-C	T1	Qsg	R	TP1	c	M3t	80	0.46	0.01	0.65	0.07	15	0	1612-13	lcp, basin
T1-100-T	T1	Qsg	R	TP1	t	W2	81	0.56	0.03	0.93	0.15	30	8	1614-16	
T1-200-C	T1	Qsg	R	TP1	c	M3t	83	0.33	0.03	0.44	0.04	12	0	1625-26	SALLAN to 12 cm
T1-200-T	T1	Qsg	R	TP1	t	W2	82	0.51	0.02	0.24	0.02	40	22	1618-21	
T2-5-C	T2	Qsg	R	TP1	c	W1d	86	0.39	0.02	0.92	0.14	23	0	1627-30	very dusty
T2-5-T	T2	Qsg	R	TP1	t	A1t	85	0.57	0.01	0.93	0.08	21	3	1632-35	trough, some grazing
T2-10-C	T2	Qsg	R	TP1	c	W1d	84	0.46	0.02	0.75	0.27	20	0	1639-42	willows to 25 cm
T2-10-T	T2	Qsg	R	TP1	t	A1t	87	0.79	0.01	NA	NA	10	63	1636-38	Dead CARAQU (lots of Daphnia)
T2-25-C	T2	Qsg	R	TP1	c	W1d	88	0.47	0.01	0.43	0.02	18	0	1643-44	hcp
T2-25-T	T2	Qsg	R	TP1	t	A1t	89	0.64	0.05	NA	NA	NA	43	1645-47	
T2-50-C	T2	Qsg	R	TP1	c	M3t	90	0.50	0.01	0.22	0.04	12	0	1648-50	hcp
T2-50-T	T2	Qsg	R	TP1	t	A1t	91	0.48	0.19	1.05	0.14	43	26	1651-53	height are above water
T2-100-C	T2	Qsg	R	TP1	c	M3t	92	0.52	0.01	0.64	0.14	16	0	1654-57	willow to 20xm
T2-100-T	T2	Qsg	R	TP1	t	A1t	93	0.38	0.14	0.52	0.06	35	24	1658-61	Flooded trough: 1/2 of plot: CALRIC-RANGME; 1/2 CARAQU-CALRIC (LAI taken in this half)
T2-200-C	T2	Qsg	R	TP1	c	M3t	95	0.54	0.01	0.47	0.11	11	0	1664-67	hcp, SALLAN to 12 cm
T2-200-T	T2	Qsg	R	TP1	t	A1t	96	0.71	0.01	1.19	0.07	22	4	1668-71	grazing by geese
T3-5-C	T3	Qti	Dlir2	TP2	c	NA	NA	NA	NA	0.92	0.14	NA	0	NA	Plot destroyed by road
T3-5-T	T3	Qti	Dlir2	TP2	t	NA	NA	NA	NA	0.93	0.08	NA	0	NA	Plot destroyed by road
T3-10-C	T3	Qti	Dlir2	TP2	c	M3d	111	0,27	0.04	0.75	0.27	5	0	1672-73	SALLAN to 21 cm
T3-10-T	T3	Qti	Dlir2	TP2	t	A1t	112	0.4	0.16	NA	NA	30	75	1674-77	1/4 of plot with CARAQU, deep water
T3-25-C	T3	Qti	Dlir2	TP2	c	M3d	113	0.16	0.06	0.43	0.02	4	0	1679-81	DRYINT, HULINT,
T3-25-T	T3	Qti	Dlir2	TP2	t	A1t	114	2.16	0.32	NA	NA	32	0	1682-84	hcp trough; transitional CARAQU,ERIANG, lots of litter

Table A2 *(continued)*

Plot ID	Transect	Plot landscape characterization[1]					NDVI		LAI			Veg height[2] (cm)	Water depth (cm)	Photo number	Notes[3]
		Surficial geology	Land-form	Surface feature	Surface-feature element	Vegetation habitat	File number	Mean	SE	Mean	SE				
T3-50-C	T3	Qti	Dlir2	TP2	c	W1d	116	0.55	0.13	0.22	0.04	16	0	1685-88	Transitional lcp
T3-50-T	T3	Qti	Dlir2	TP2	t	A1t	115	0.54	0.07	1.05	0.14	36	27	1689-91	lots of dead CARAQU, some CALRIC; 10 cm H2O
T3-100-C	T3	Qti	Dlir2	TP2	c	W1d	117	0.32	0.1	0.64	0.14	7	0	1694-98	Transitional lcp, lots of ERIANG, CARCAP, DRYINT, SALRET, CARSCI, HULINT, PEDLAN, POLVIV
T3-100-T	T3	Qti	Dlir2	TP2	t	A1t	118	0.54	0.07	0.52	0.06	28	26	1703-07	lots of dead CARAQU, some CALRIC; about 20% open water
T4-5-C	T4	Qti	DLir2	TP1	c	NA	119	0.32	0.10	0.49	0.8	31	27	1737	CARAQU
T4-5-T	T4	Qti	DLir2	TP1	t	NA	120	-0.26	0.20	0.07	0	23	62	1738-40	mostly water, sparse CARAQU, many dead carices. grazed
T4-10-C	T4	Qti	DLir2	TP1	c	M3d	122	0.70	0.03	0.56	0.08	38	25	1745-48	CARAQU
T4-10-T	T4	Qti	DLir2	TP1	t	A1t	121	-0.86	0.00	0	0	0	89	1741-43	Deep water >100 cm, no vegetation
T4-25-C	T4	Qti	DLir2	TP1	c	M3d	NA	NA	NA	NA	NA	NA	24	NA	plot not found
T4-25-T	T4	Qti	DLir2	TP1	t	A1t	NA	NA	NA	NA	NA	NA	92	NA	plot not found
T4-50-C	T4	Qti	DLir2	TP1	c	W1d	124	0.64	0.03	0.76	0.07	31	26	1752-54	CARAQU, SCOSCO
T4-50-T	T4	Qti	DLir2	TP1	t	A1t	123	0.63	0.02	0.58	0.06	35	44	1755-57	CARAQU
T4-100-C	T4	Qti	DLir2	TP1	c	W1d	126	0.72	0.02	0.96	0.03	31	19	1761-64	CARAQU, water about 20 cm deep
T4-100-T	T4	Qti	DLir2	TP1	t	A1t	125	0.63	0.03	0.83	0.07	40	27	1758-60	CARAQU. water 70 m deep
T5-5-C	T5	Qti	DLir2	TP1	NA	Heavily disturbed	NA	NA	NA	NA	NA	NA	NA	NA	No data, heavily disturbed area associated with fiber optic cables
T5-5-T	T5	Qti	DLir2	TP1	NA		NA	NA	NA	NA	NA	NA	NA	NA	
T5-10-C	T5	Qti	DLir2	TP1	NA		NA	NA	NA	NA	NA	NA	NA	NA	
T5-10-T	T5	Qti	DLir2	TP1	NA		NA	NA	NA	NA	NA	NA	NA	NA	
T5-25-C	T5	Qti	DLir2	TP1	c	M3t	105	0.60	0.02	0.54	0.08	18	0	1768-69	lcp, center, SALLAN to 22 cm; transitional to U4 with willows
T5-25-T	T5	Qti	DLir2	TP1	t	A1t	106	0.69	0.01	1.88	0.27	30	0	1770-73,76	lcp trough, CARAQU, ERIANG, lots of litter
T5-50-C	T5	Qti	DLir2	TP1	c	M3t	108	0.58	0.01	1.32	0.07	23	0	1782-84	ERIANG, SALLAN to 28 cm, lots of litter
T5-50-T	T5	Qti	DLir2	TP1	t	M2t	107	0.62	0.02	0.95	0.11	25	0	1777-80	Trough, sides are U4, crack above ice wedge – M2, mossy, DREPSP, no water within the plot
T5-100-C	T5	Qti	DLir2	TP1	c	M3t	110	0.57	0.02	0.71	0.09	16	0	1784-89	Flat-centered polygon not rims, previous lcp; SALLAN to 15 cm
T5-100-T	T5	Qti	DLir2	TP1	t	A1t	109	0.63	0.01	2.25	0.08	28	11	1790-96	Lots of dead sedges, CARAQU, remnant SALLAN, SALRIC, considerable water beneath the litter

Notes: [1] Plot landscape characterization codes are in Table 1. [2] Vegetation heights in water were measured above the water level. [3]Colleen site: Dust is less on the T1 side of road; Salix lanata (SALLAN) is much more abundant at Colleen site than at NIRPO, especially within approximately 50 m of the road. Transect T2: Troughs seem wider and more difficult to cross than during 2022 visit. Airport site: Transect T3 is heavily dusted and strongly eroded with mainly dry vegetation on polygon centers) and deeply eroded troughs; movie of Transect 3 taken from road along river and at east end of transect (Walker photos: IMG_1727, 38.8 mb). On transect T4 water is continuous over the who entire area, and generally deeper than 20 cm except in troughs, where it is much deeper; few gravel bars above the water table, where gravel was displaced from the access road during the 2015 flood; Deeply eroded troughs; cover of CARAQU is much more homogeneous than in 2015. Abbreviations in notes: low-center polygon (lcp), high-center polygon (hcp), 6-letter taxon codes (CARAQU, CALRIC, ERIANG, etc.) based on first three letters of plant's genus and species.

ALASKA GEOBOTANY CENTER

The Alaska Geobotany Center (AGC) is dedicated to understanding northern ecosystems through the use of geographic information systems, remote sensing, field experiments, and cooperative team research projects. We share a commitment to excellence in field research and teaching with the goal of inspiring an appreciation of northern ecosystems and making our research and teaching relevant to societal issues and concerns, particularly issues relevant to the state of Alaska.

Alaska Geobotany Center
Institute of Arctic Biology
University of Alaska Fairbanks

P.O. Box 757000
Fairbanks, AK 99775-7000
Phone (907) 474-2459

www.geobotany.uaf.edu